Translational Research 272 (2024) 95–110

Contents lists available at ScienceDirect

Translational Research

journal homepage: www.elsevier.com/locate/trsl

A proteomic approach supports the clinical relevance of TAT-Cx43$_{266-283}$ in glioblastoma

Sara G. Pelaz [a,1,**], Raquel Flores-Hernández [a], Tatjana Vujic [b,c], Domitille Schvartz [b,d], Andrea Álvarez-Vázquez [a], Yuxin Ding [a], Laura García-Vicente [a], Aitana Belloso [a], Rocío Talaverón [a], Jean-Charles Sánchez [b], Arantxa Tabernero [a,*]

[a] Instituto de Neurociencias de Castilla y León (INCYL), Departamento de Bioquímica y Biología Molecular, Universidad de Salamanca, Instituto de Investigación Biomédica de Salamanca (IBSAL), Calle Pintor Fernando Gallego 1, Salamanca, 37007, Spain
[b] Department of Medicine, University of Geneva, 1211, Geneva, Switzerland
[c] University Center of Legal Medicine, Lausanne-Geneva, Lausanne University Hospital and University of Lausanne, Geneva University Hospital and University of Geneva, Lausanne Geneva, Switzerland
[d] University of Geneva, Faculty of Medicine, Proteomics Core Facility, Geneva, Switzerland

ARTICLE INFO

Keywords:
Glioblastoma
Brain tumors
Proteomics
Src
Connexin
Cell-penetrating peptides

ABSTRACT

Glioblastoma (GBM) is the most frequent and aggressive primary brain cancer. The Src inhibitor, TAT-Cx43$_{266-283}$, exerts antitumor effects in in vitro and in vivo models of GBM. Because addressing the mechanism of action is essential to translate these results to a clinical setting, in this study we carried out an unbiased proteomic approach. Data-independent acquisition mass spectrometry proteomics allowed the identification of 190 proteins whose abundance was modified by TAT-Cx43$_{266-283}$. Our results were consistent with the inhibition of Src as the mechanism of action of TAT-Cx43$_{266-283}$ and unveiled antitumor effectors, such as p120 catenin. Changes in the abundance of several proteins suggested that TAT-Cx43$_{266-283}$ may also impact the brain microenvironment. Importantly, the proteins whose abundance was reduced by TAT-Cx43$_{266-283}$ correlated with an improved GBM patient survival in clinical datasets and none of the proteins whose abundance was increased by TAT-Cx43$_{266-283}$ correlated with shorter survival, supporting its use in clinical trials.

Introduction

Glioblastoma (World Health Organization grade 4 glioma, GBM) [1] is the most common and aggressive primary brain cancer. To date, GBM remains one of the most incurable forms of cancer: despite considerable effort, no therapeutic progress has significantly improved survival in the last decades (https://seer.cancer.gov). Thus, GBM median overall survival is approximately 15–18 months with standard-of-care consisting of surgery, radiotherapy, and temozolomide, [2] and 20.9 months with the addition of tumor-treating fields.[3] A subset of cells within GBMs, termed glioblastoma stem cells (GSCs), are self-renewing, tumor-initiating, and therapy-resistant.[4,5] They are considered responsible for tumor recurrence, which is the primary cause of treatment failure and death in GBM patients; therefore, GSCs constitute a relevant target in GBM treatment.

GBM cells, and particularly GSCs, exhibit high c-Src activity,[6] which is involved in the transforming phenotype of astrocytomas.[7] c-Src (*SRC*), the first oncogene ever identified,[8] is a non-receptor tyrosine kinase that participates in signaling pathways controlling a diverse spectrum of biological events. Src integrates cell signals to function as both effector and regulator of a plethora of receptors, enabling the crosstalk between different signaling pathways. This integrative role of Src is context-dependent; hence, the Src-induced response to a specific stimulus may act through different downstream pathways across cell states and types. Src activity positively modulates proliferation, differentiation, survival, angiogenesis, integrin signaling, invasion, migration and metabolic plasticity (reviewed in [9]). Src acts as a proto-oncogene, playing key roles in the development of several types of tumors, including GBM.[10] Indeed, Src activity correlates with shorter survival in GBM patients,[11] who show the highest overactivation of Src across many tumor types.[9]

* Corresponding author at: Instituto de Neurociencias de Castilla y León (INCYL), Calle Pintor Fernando Gallego 1, Salamanca, 37007, Spain.
** Co-corresponding author.
E-mail addresses: sgutierrezpelaz@mednet.ucla.edu (S.G. Pelaz), ataber@usal.es (A. Tabernero).
[1] Current affiliation: Department of Physiology, University of California, Los Angeles (UCLA), CA, USA.

https://doi.org/10.1016/j.trsl.2024.06.001
Received 12 March 2024; Received in revised form 18 May 2024; Accepted 1 June 2024
Available online 12 June 2024

Despite the prominent role of Src in GBM,[12,13] the ATP-competitive Src inhibitor, Dasatinib, failed to improve the overall survival of recurrent GBM patients in clinical trials.[14,15] A mechanism for drug-resistance, [16] side effects related to the conserved ATP-binding site, incomplete knowledge of the mechanism of action together with reduced ability to reach GBM cells and lack of predictive response biomarkers have been proposed among the causes of the failure of ATP-competitive inhibitors in clinical results [17]. To overcome these problems, new and appealing strategies in the development of Src inhibitors are emerging, such as the cell-penetrating peptide, TAT-Cx43$_{266-283}$. Connexin43 (Cx43), the gap junction forming protein, physiologically inhibits Src activity [18] through the recruitment of Src together with its endogenous inhibitors, CSK and PTEN.[19] The Cx43 mimetic peptide, TAT-Cx43$_{266-283}$, recapitulates this mechanism because it acts as a docking platform for Src, CSK and PTEN, and consequently inhibits Src activity.[19] TAT-Cx43$_{266-283}$ inhibits the oncogenic activity of Src and exerts important antitumor effects in several preclinical models of GBM in vitro, ex vivo, and in vivo, including freshly removed surgical specimens from patients.[20,21] Tumour cell proliferation, survival, migration, invasion, metabolic plasticity and autophagy are impaired by TAT-Cx43$_{266-283}$, and GBM-bearing mice treated with TAT-Cx43$_{266-283}$ display enhanced survival.[11,22,23] One of the main advantages of the Src inhibitor TAT-Cx43$_{266-283}$ is that its effects are specific for the GSC subpopulation, with virtually no effects on healthy brain cells.[23] Indeed, the toxicity of TAT-Cx43$_{266-283}$ for neurons and astrocytes is much lower than that exerted by Dasatinib.[22]

To deepen our understanding of the antitumor TAT-Cx43$_{266-283}$ mechanism(s) of action, we carried out an unbiased proteomic approach to identify acute biological responses of human GSCs treated in vitro with TAT-Cx43$_{266-283}$. As a negative control we selected TAT-Cx43$_{274-291}$ because it does not recruit Src inhibitors or exert antitumor effects.[11,19,20] Data-independent acquisition mass spectrometry (DIA-MS) was chosen because it allows for deep and unbiased proteome characterization and quantification, including low-abundance proteins, with high reproducibility and accuracy. Another major advantage of DIA-MS is that it is label-free (i.e., it does not require tags such as isobaric labels or radioactive amino acids), contrary to other classic quantitative shotgun proteomics approaches.[24,25] First, several steps were carried out to ensure quality control of the samples and the DIA-MS proteomics. Then, we studied the top modulated pathways and proteins to investigate the impact of TAT-Cx43$_{266-283}$ on GSC proteome and biology. We compared our results with publicly available GBM patient data to study the potential clinical relevance of the proteome modulation exerted by TAT-Cx43$_{266-283}$. Finally, we validated some of the results by western blotting and immunofluorescence in vitro and in vivo. Our study unveils crucial proteins that are either candidates or confirmed effectors of the antitumor effect of TAT-Cx43$_{266-283}$.

Results

Data-independent acquisition mass spectrometry for proteome characterization of TAT-Cx43$_{266-283}$ effect in G166 GSCs

For the DIA-MS experiments, human GSCs (G166) were treated with either TAT-Cx43$_{266-283}$ or TAT-Cx43$_{274-291}$ (as a negative control). The negative control peptide TAT-Cx43$_{274-291}$, another Cx43-based cell-penetrating peptide, shares with TAT-Cx43$_{266-283}$ its total number of residues and the presence of the SH3 binding motif. However, unlike TAT-Cx43$_{266-283}$, TAT-Cx43$_{274-291}$ does not recruit c-Src's inhibitors and does not display antitumor activity.[20] G166 GSCs were seeded in biological and technical triplicates, treated with TAT-Cx43$_{266-283}$ or TAT-Cx43$_{274-291}$ for 24 h at 50 μM (Supp. Fig. 1A), enzymatically dissociated and centrifuged, and the resulting pellets were lyophilized. Before MS analysis, sample quality was investigated by one-dimension SDS-PAGE followed by silver nitrate staining, and subsequently one technical replicate from each condition in each biological replicate was selected for DIA-MS (Supp. Fig. 1B). Proteins from the selected samples were extracted, digested and desalted for MS injection (see Methods).

DIA-MS allowed the quantification of 72,486 peptides corresponding to 6,457 proteins. Reproducibility across technical and biological replicates was high as indicated by a median Pearson correlation coefficient of precursor intensities of 0.98 (Fig. 1A). In G166 GSCs treated with TAT-Cx43$_{266-283}$, statistical analysis revealed a significant change in abundance (false discovery rate [FDR] < 0.05, absolute fold change [$|FC|$] > 1.2) for 190 proteins, whereas for TAT-Cx43$_{274-291}$ this number was 337 (Fig. 1B and C, Supp. Fig 1C, and Tables S1 and S2). The abundance of 96 proteins was found to be similarly modified by both treatments (Fig. 1B and Supp. Fig. 1D). This was expected, as the Cx43 sequence contained in TAT-Cx43$_{274-291}$ includes known functional motifs such as the SH3 binding motif (shared with TAT-Cx43$_{266-283}$) or a NEDD4 binding motif (unique to TAT-Cx43$_{274-291}$).[26,27] To explore the changes in protein abundance variation across samples, we performed a principal component analysis (PCA), which can determine the principal axes of abundance variation. The PCA of the proteins whose abundance was significantly modified in at least one of the treatments showed that the first component accounted for most of the variability (more than 40%) and grouped the samples according to treatment (same-treatment samples, graphed in the same color, were grouped together across the PC1 axis, i.e., were vertically grouped), while the smaller, second component grouped the samples according to biological replicate (same-replicate samples, identified by the same number, were grouped together across the PC2 axis, i.e., were horizontally grouped) (Fig. 1D). Therefore, DIA-MS of GSCs unveiled a reproducible change in abundance for 190 proteins following TAT-Cx43$_{266-283}$ treatment.

Top biological pathways modulated by TAT-Cx43$_{266-283}$

To interrogate the biological meaning of the proteins whose abundance was modulated by the treatments, we manually interrogated the results and also used several pathway analysis tools: MetaCore™ (Clarivate Analytics), a proprietary software with a manually curated database containing signaling and metabolic pathways and other relevant biological data; Metascape [28] (https://metascape.org), which combines over 40 independent knowledgebases; and the String database [29] (https://string-db.org), which aims to integrate all known and predicted associations between proteins, and includes physical interactions as well as functional associations. Below, we describe several relevant biological pathways putatively modified by TAT-Cx43$_{266-283}$ and TAT-Cx43$_{274-291}$ treatment in GSCs (Fig. 2 and Supp. Fig. 2). Although the abundance of some proteins modified by both treatments might be relevant for the mechanism of action of TAT-Cx43$_{266-283}$, here we focused on proteins whose abundance was uniquely modulated by this peptide.

Cytoskeleton and membrane dynamics

Among the top processes modulated uniquely by TAT-Cx43$_{266-283}$ were actin filament-based process, cell junction organization and cell morphogenesis (Fig. 2A). Indeed, treatment with TAT-Cx43$_{266-283}$, but not with TAT-Cx43$_{274-291}$, reduced the levels of crucial cytoskeletal proteins involved in cell adhesion, signal transduction and membrane dynamics, such as catenin alpha1 (CTNNA1), catenin delta1 or p120 (CTNND1), dystonin (DST), gelsolin (GSN), and talin-1 (TLN1) (Fig. 2B). Moreover, other proteins that regulate the assembly and membrane binding of the actin cytoskeleton, such as alpha-actinin-1 (ACTN1), 4 (ACTN4), cofilin-1 (CFL1), inverted formin-2 (INF2), IQ Motif Containing GTPase Activating Protein 1 (IQGAP1) and nesprin-2 (SYNE2), and proteins that localize to focal adhesions, such as paxillin (PXN), were less abundant in GSCs after TAT-Cx43$_{266-283}$ or TAT-Cx43$_{274-291}$ treatment (Fig. 2B).

Treatment with TAT-Cx43$_{274-291}$, unlike TAT-Cx43$_{266-283}$, does not reduce GSC survival,[20] but it did induce a phenotype where cells reorganize into patches in the culture dish (Supp. Fig. 1A). In agreement, the

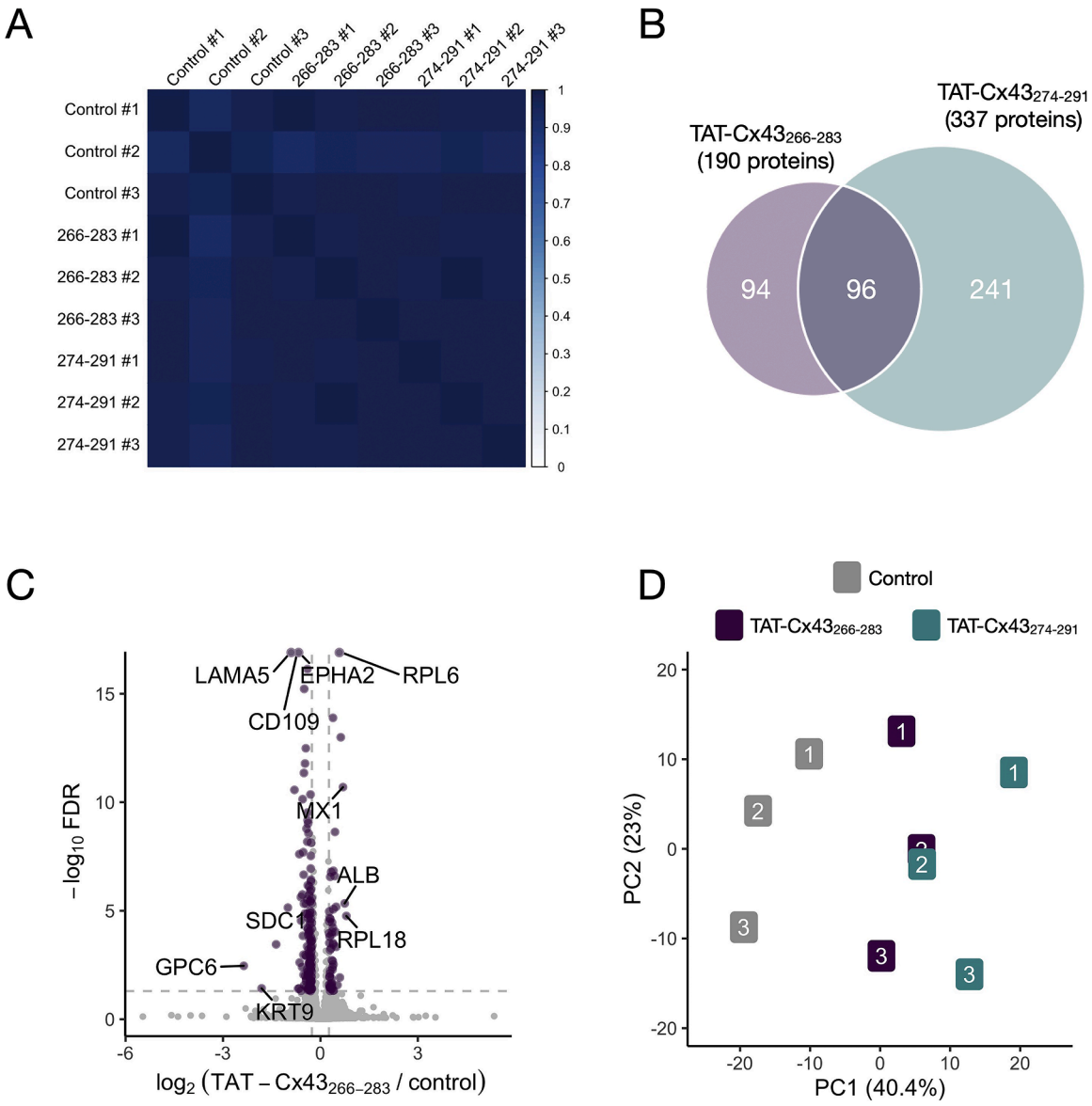

Fig. 1. DIA-MS of GSCs proteomics.
A. Pearson correlation coefficients of precursor intensities across samples.
B. Venn diagram of significantly changing proteins for each treatment [FDR < 0.05, |FC| > $\log_2(1.2)$].
C. Volcano plot highlighting proteins with significant change in abundance [FDR < 0.05, |FC| > $\log_2(1.2)$] after TAT-Cx43$_{266\text{-}283}$ treatment. Proteins with the highest |FC| values are indicated by name.
D. Principal component analysis (PCA) of the proteins whose abundance was significantly modified in at least one of the treatments.

levels of some cytoskeletal proteins were found to be increased only upon TAT-Cx43$_{274\text{-}291}$ treatment. This is the case for ezrin (EZR), radixin (RDX) and moesin (MSN), the three members of the so-called ERM protein family, which crosslink actin filaments to the plasma membrane [30] and can bind and stabilize microtubules [31] (Fig. 2B). The same was true for other cytoskeleton-related proteins, namely Rac1 (RAC1), which, among other functions, is an upstream regulator of cytoskeletal organization, and vinculin (VCL), an actin-binding protein enriched in focal adhesions and adherens junctions (Fig. 2B). On the other hand, another important cytoskeletal protein, vimentin (VIM), was found to increase its abundance in response to TAT-Cx43$_{266\text{-}283}$ or TAT-Cx43$_{274\text{-}291}$ (Fig. 2B). Vimentin is part of the intermediate filaments, a different cytoskeletal entity from actin filaments, and helps cells maintain their shape.[32] Finally, many of the aforementioned proteins were found to functionally and/or physically interact according to existing literature (Fig. 2C), further reinforcing the idea that TAT-Cx43$_{266\text{-}283}$ treatment can modulate cytoskeletal and membrane dynamics.

Extracellular matrix signaling: laminins and integrins

Among the top pathways modulated by TAT-Cx43$_{266\text{-}283}$ were laminin interactions and cell-cell communication (Fig. 2A). Laminins are a family of glycoproteins found in the basal membrane of the extracellular matrix. Laminin isoforms consist of an heterotrimer made of 3 laminin subunits: alpha, beta and gamma. Laminin 11 is formed by the alpha-5 (LAMA5), beta-2 (LAMB2) and gamma-1 (LAMC1) subunits,[33] all of which were found to be less abundant after TAT-Cx43$_{266\text{-}283}$ treatment, whereas TAT-Cx43$_{274\text{-}291}$ only reduced the levels of laminin-alpha-5 and gamma-1 (Fig. 2A and B). Laminins can act as ligands for integrins, which are cell membrane heterodimeric proteins that facilitate cell-cell and cell-extracellular matrix interactions and can trigger signaling transduction pathways, including, most notably for this study, c-Src

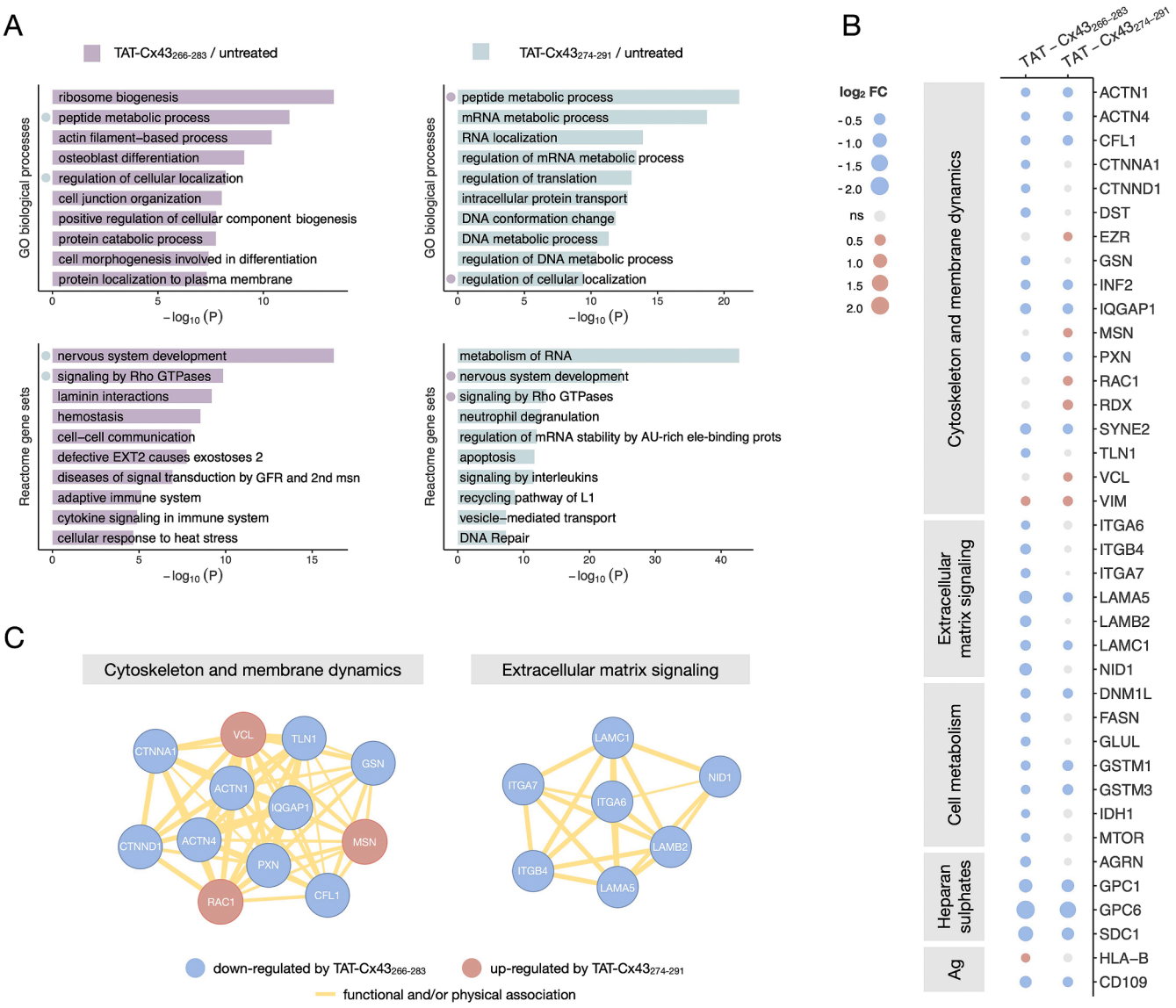

Fig. 2. Top biological pathways and proteins modulated by TAT-Cx43$_{266-283}$.
A. The ten most significant enriched gene ontology biological processes (GO) (top) and Reactome gene sets (bottom) for the proteins changing after treatment with TAT-Cx43$_{266-283}$ (left, purple) or TAT-Cx43$_{274-291}$ (right, blue) using Metascape (Tables S6 and S7). Blue and purple circles show common processes.
B. DIA-MS-based relative abundance of selected proteins discussed in the main text. Blue, red, and gray circles indicate significant reduction, increase and not significant changes, respectively. The size of the circles corresponds to log2FC, as indicated in the figure.
C. STRING analysis map of functional and/or physical association of proteins participating in cytoskeleton and membrane dynamics (left) and extracellular matrix signaling (right).

related pathways.[34,35] According to our results, integrin-alpha-6 (ITGA6), integrin-alpha-7 (ITGA7), and integrin-beta-4 (ITGB4) were less abundant after TAT-Cx43$_{266-283}$ treatment but not after TAT-Cx43$_{274-291}$ treatment (Fig. 2B). Interestingly, laminin 11 (LAMA5, LAMB2 and LAMC1) can bind and activate the integrin heterodimer alpha-6/beta-4,[36] and all these proteins were less abundant after TAT-Cx43$_{266-283}$ treatment (Fig. 2B and C). Moreover, nidogen-1 (NID1), which connects the networks formed by laminin and its partners, was also less abundant following TAT-Cx43$_{266-283}$ treatment (Fig. 2B and C). Together, these changes suggest that TAT-Cx43$_{266-283}$ may modulate the laminin-integrin axis in GSCs (Fig. 2B and C).

Cell metabolism

We have previously found that TAT-Cx43$_{266-283}$ impairs glucose metabolism and metabolic plasticity in GSCs, and that mitochondrial localization, structure and function are compromised upon TAT-Cx43$_{266-283}$ treatment.[23] Our DIA-MS data revealed a possible molecular modulator of these mitochondrial effects, as dynamin-related protein 1 (Drp-1, *DNM1L*), a protein that regulates mitochondrial fission, was less abundant in TAT-Cx43$_{266-283}$ and in TAT-Cx43$_{274-291}$-treated samples (Fig. 2B). Moreover, TAT-Cx43$_{266-283}$ decreased the abundance of proteins involved in the regulation of lipid metabolism (fatty acid synthase, FASN), amino acid metabolism (mammalian target of rapamycin, MTOR; glutamate-ammonia ligase, GLUL, which belongs to the glutamine synthetase family) and the tricarboxylic acid cycle (isocitrate dehydrogenase 1, IDH-1). Treatment with either peptide decreased the abundance of two isoforms of the redox balance regulator glutathione S-transferase (GSTM1, GSTM3). Together, these new data further support the role of TAT-Cx43$_{266-283}$ on GSC metabolism and metabolic plasticity.[23]

Heparan sulphate proteoglycans

Proteoglycans are proteins glycosylated with glycosaminoglycans (amino-polysaccharides) that are present in the cell membrane as well as the extracellular matrix. Heparan sulphate proteoglycans (HSPGs), one of several types of proteoglycans, regulate a wide range of biological functions, such as development, growth factor signaling (where they act as co-receptors), angiogenesis and cell adhesion.[37,38] HSPGs interact with growth factors through the negatively charged heparan sulphate molecules, and with intracellular proteins - such as c-Src, in the case of syndecans,[37] or cytoskeletal proteins - through their cytoplasmic domains, hence acting as growth factor co-receptors. Indeed, growth-factor-dependent signaling mediated by HSPGs facilitates primary tumor growth and angiogenesis.[39] Four HSPGs were less abundant after TAT-Cx43$_{266-283}$ treatment: agrin (AGRN), glypican-1 (GPC1), glypican-6 (GPC6) and syndecan-1 (SDC1) (Fig. 2B). The abundance of glypican-1, glypican-6 and syndecan-1 were also reduced by TAT-Cx43$_{274-291}$, while agrin was specifically down-regulated by TAT-Cx43$_{266-283}$.

Antigen presentation and immune surveillance

As shown in the Reactome gene sets (Fig. 2A), "adaptative immune system" and "cytokine signaling in immune system" are among the top pathways affected specifically by TAT-Cx43$_{266-283}$ when compared to untreated cells. GBM has long been studied as a paradigm of cancer-induced immune evasion.[40,41] One putative mechanism involves GSC expressing decreased levels of human leukocyte antigen class I molecules (HLA, genetically encoded by the major histocompatibility complex class I, *MHC*).[42-44] Interestingly, HLA-B (one of the 3 classic HLA class I proteins) was more abundant in GSCs after TAT-Cx43$_{266-283}$ treatment, but not after TAT-Cx43$_{274-291}$ treatment (Fig. 2B). Conversely, DIA-MS revealed that both peptides reduced the abundance of CD109, a glycosyl-phosphatidyl-inositol-linked cell surface antigen (Fig. 2B) associated with the GBM cancer-initiating population from the tumor core and therapy resistance, and negatively correlated with patient survival.[45-49]

Clinical relevance of proteins modulated by TAT-Cx43$_{266-283}$ in GBM

In order to explore the clinical relevance of the proteins modulated by TAT-Cx43$_{266-283}$ in GSCs in the context of GBM, we compared the list of proteins whose abundance was modified by the peptide to two other datasets resulting from analyses of patient data by The Pathology Atlas [50] (https://www.proteinatlas.org/humanproteome/pathology/glioma). The first dataset lists RNAs found to be elevated in GBM compared to other cancers (Table S3), the other dataset lists RNAs found to correlate with unfavorable prognosis in GBM (Table S4). Unfortunately, we are unaware of the existence of similarly sized datasets containing protein levels instead of mRNA levels, and hence we carried out the analyses using mRNA data.

Clusterin (CLU) and integrin-alpha-7 (ITGA7): gene products elevated in GBM and down-regulated by TAT-Cx43$_{266-283}$

Of the 682 mRNAs elevated in GBM compared to other cancers according to The Pathology Atlas (Table S3), the protein products of 82 of them (12%) were identified in our DIA-MS analysis (Fig. 3A). Three of them were less abundant after treatment with TAT-Cx43$_{266-283}$ in G166 GSCs: clusterin (*CLU*, also known as ApoJ), integrin-alpha-7 (*ITGA7*) and tubulin-alpha-1a (*TUBA1A;* this protein was also down-regulated by TAT-Cx43$_{274-291}$) (Fig. 3B). None of the remaining 79 proteins were found to have significantly different levels across treatments.

To evaluate whether the mRNAs of these 3 proteins, clusterin, integrin-alpha-7 and tubulin-alpha-1a, were also up-regulated in GBM compared to other gliomas, we analyzed mRNA levels with GlioVis [51] (http://gliovis.bioinfo.cnio.es/), a web-based tool that allows for easy and intuitive exploration of mRNA levels data in glioma patients. Out of the several datasets available in GlioVis, we chose the CGGA,[52] the Rembrandt [53] and the TCGA GBM [54] and LGG [55] datasets (https://www.cancer.gov/tcga) for our analyses, as they contained the highest number of GBM patients and included samples from low-grade as well as high-grade glioma (the Rembrandt dataset also includes non-tumor tissue). Analysis of the levels of *CLU, ITGA7* and *TUBA1A* mRNA levels across glioma histology in the 3 datasets revealed enhanced levels of the 3 genes in GBM compared to oligodendrogliomas or astrocytomas, low-grade gliomas with a better prognosis than GBM (Fig. 3C). Consequently, lower levels of any of these 3 genes correlated with better survival in glioma patients (Supp. Fig. 3). It must be noted that although reduced levels of *CLU, ITGA7* and *TUBA1A* could be the cause of improved survival, it is also possible that tumor grade contributes to better survival independently of the levels of these genes, as low-grade glioma patients have better survival rates than high-grade glioma patients. To exclude the possible role of tumor grade as a confounding variable, we performed the survival analysis with only GBM patients. Lower levels of *TUBA1A* mRNA were associated with higher survival only in 1 of the 3 datasets, and lower levels of *CLU* or *ITGA7* mRNA were associated with higher survival in all 3 datasets tested (Fig. 3D), suggesting that reduction of clusterin or integrin-alpha-7 protein levels promoted by TAT-Cx43$_{266-283}$ might provide a clinical improvement for GBM patients.

The abundance of unfavorable prognostic gene products in GBM was not increased by TAT-Cx43$_{266-283}$

Importantly, of the aforementioned 82 proteins identified in our DIA-MS analysis (Fig. 3A) corresponding to mRNAs elevated in GBM compared to other cancers according to The Pathology Atlas (Table S3), we found that none of these proteins was more abundant after TAT-Cx43$_{266-283}$ treatment (Table S1). In the same line, The Pathology Atlas identified 201 genes (Table S4) for which higher mRNA levels correlated with shorter survival in patients from their TCGA GBM subset. We identified the protein products of 70 of these 201 genes in our GSCs samples (35%), and both TAT-Cx43$_{266-283}$ and TAT-Cx43$_{274-291}$ significantly decreased the protein abundance of 2 of them: paxillin (PXN) and syndecan-1 (SDC1) (Fig. 4A and B). Importantly, TAT-Cx43$_{274-291}$ decreased the levels of the favorable protein cytochrome P450 oxidoreductase (POR) but increased the levels of the unfavorable protein disulfide-isomerase A4 (PDIA4) (Table S2), however, TAT-Cx43$_{266-283}$ did not increase the abundance of any unfavorable GBM genes (Table S1),

Although the abundance of paxillin and syndecan-1 were decreased by both TAT-Cx43$_{266-283}$ and TAT-Cx43$_{274-291}$, they might contribute to the antitumor effects of TAT-Cx43$_{266-283}$, in combination with specific effectors of this peptide. In fact, the analysis using GlioVis [51] revealed increased levels of *PXN* and *SDC1* mRNA in GBM compared to lower grade gliomas (Fig. 4C). Consequently, higher levels of *PXN* or *SDC1* correlated with higher mortality in glioma patients in the three datasets analyzed (Supp. Fig. 3). When the analysis was restricted to GBM patients, we found a consistent association of lower *PXN* or *SDC1* mRNA levels with lower mortality (Fig. 4D) in all three datasets.

Validation of DIA-MS results: HLA-B, laminin and p120

As described, DIA-MS revealed that TAT-Cx43$_{266-283}$ treatment altered important proteins in human GSCs (Table S1). Among them, three proteins (HLA-B, laminin and p120), whose abundance was modified specifically by TAT-Cx43$_{266-283}$ and belonging to different biological pathways, were selected for validation by western blotting (Fig. 5A-E). Fig. 5D and E show representative cropped blots and quantifications, while Supp. Fig. 4 shows the uncropped triplicate blots using aliquots from the same three independent experiments analyzed by DIA-MS.

Intriguingly, our proteomics study unveils a putative role for TAT-Cx43$_{266-283}$ in the immune response elicited by GSCs. DIA-MS shows that HLA-B (a classic HLA class I protein) was more abundant in GSCs

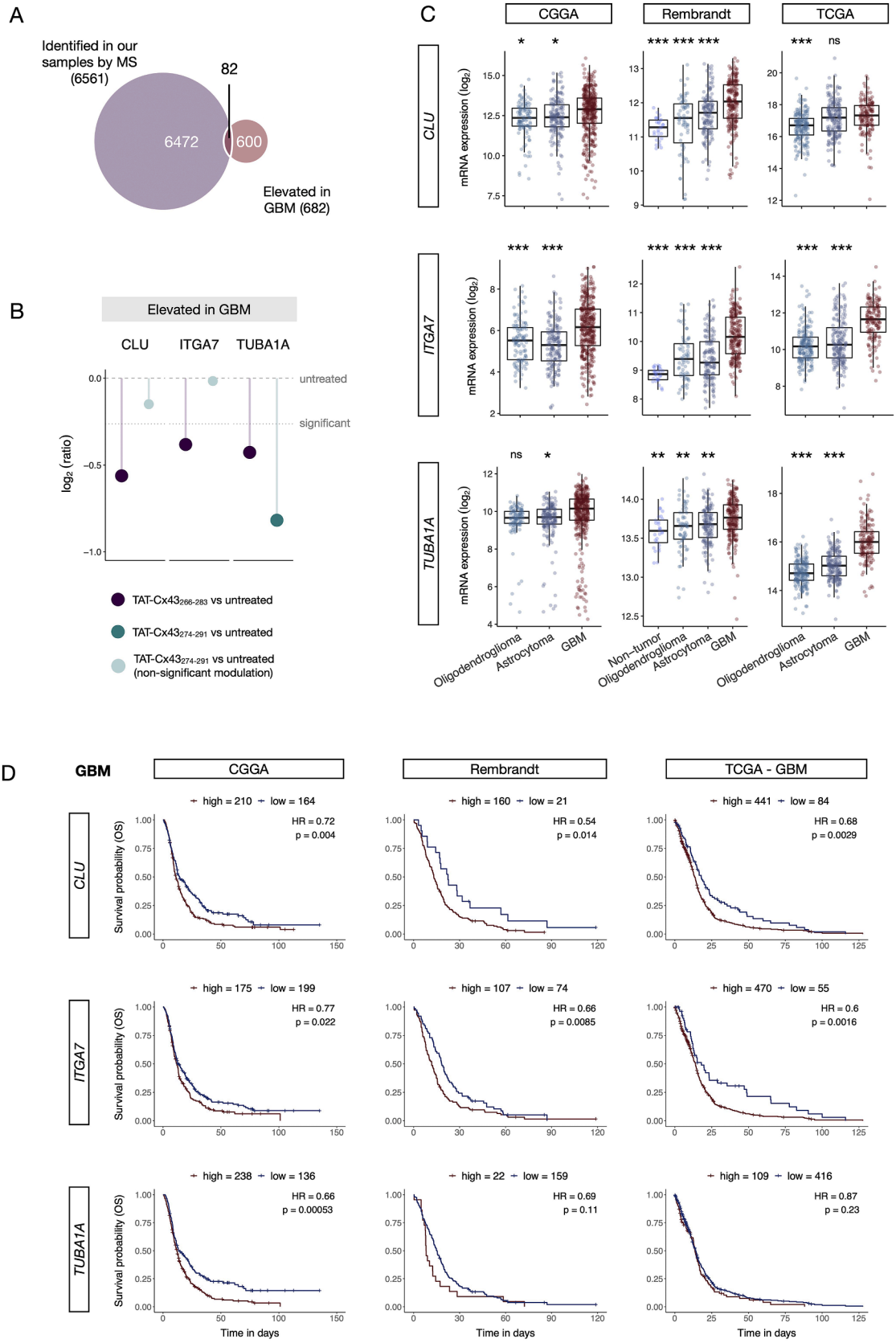

(caption on next page)

Fig. 3. TAT-Cx43$_{266-283}$ decreases the abundance of three proteins specifically elevated in GBM: clusterin, integrin-α-7 and tubulin-α-1a. Proteins identified in our MS analysis were compared to genes whose mRNA level was found to be elevated in GBM by the Pathology Atlas.
A. Venn diagram of proteins identified in our MS analysis and genes elevated in GBM.
B. The abundance of three proteins, clusterin (*CLU*), integrin-α-7 (*ITGA7*) and tubulin-α-1a (*TUBA1A*), was significantly reduced by TAT-Cx43$_{266-283}$ in GSCs. Tubulin-α-1a (*TUBA1A*), was also significantly reduced by TAT-Cx43$_{274-291}$.
C. mRNA expression levels of *CLU, ITGA7* and *TUBA1A* across glioma histology in 3 datasets. The lower and upper hinges correspond to the first and third quartiles (the 25th and 75th percentiles), the central line corresponds to the median, and the whiskers extend from the first or third quartile hinge to the largest (first quartile hinge) or smallest (third quartile hinge) value within 1.5 times the inter-quartile range. $*P < 0.05$, $**P < 0.01$, $***P < 0.001$, ns: not significant vs GBM (Tukey's Honest Significant Difference).
D. Kaplan-Meier curves of GBM patient survival associated with high or low mRNA levels of the indicated genes in 3 datasets. *P* values were obtained with the log-rank test.

after TAT-Cx43$_{266-283}$ treatment, but not significantly so after TAT-Cx43$_{274-291}$ treatment (Fig. 5A). Western blot analyses showed that HLA-B protein levels were increased by TAT-Cx43$_{266-283}$ when compared to control in G166 GSCs (although not statistically significant, Fig. 5D and E, and Supp. 4C). This finding suggests that increased levels of HLA-B in TAT-Cx43$_{266-283}$-treated GSCs are not merely a response elicited by exposure to any exogenous cell-penetrating peptide, but a specific response induced by TAT-Cx43$_{266-283}$.

To validate the effect of TAT-Cx43$_{266-283}$ on extracellular matrix signaling (Fig. 5B), laminin was selected and analyzed by western blotting. Our results supported that laminin protein levels were reduced by TAT-Cx43$_{266-283}$ when compared to control in G166 GSCs (although not statistically significant, Fig. 5D and E, and Supp. Fig. 4B). Given that the molecular weights without post-translational modification for LAMA5, LAMB2 and LAMC1 are 399,74, 195,98 and 177,60 kDa, respectively,[56] the main subunit found by western blotting at 250 kDa (Fig. Supp. 4B) likely corresponds to LAMB2. Therefore, both DIA-MS and western blotting show the decrease in protein level of the β2 subunit of laminin 11, LAMB2, by TAT-Cx43$_{266-283}$ in GSCs. p120 catenin (CTNND1), a classic Src substrate,[57] was selected for validation because it plays a crucial role in cell-cell adhesion and signal transduction [58] and binds to cadherins to regulate cytoskeletal reorganization through Rho GTPases.[59] DIA-MS shows that TAT-Cx43$_{266-283}$ significantly reduced p120 catenin levels, while TAT-Cx43$_{274-291}$ had no statistically significant effect (Fig. 5C). Western blotting of p120 catenin in G166 GSCs confirmed the significant decreased abundance in TAT-Cx43$_{266-283}$--treated cells (Fig. 5D and E, and Supp. Fig. 4A).

DIA-MS unveiled the participation of p120 in the antitumor effect of TAT-Cx43$_{266-283}$

Because an important antitumor effect of TAT-Cx43$_{266-283}$ in vitro and in vivo is the impairment of migration and invasion of GSCs [20] and p120 catenin plays a pivotal role in diffuse glioma cell infiltration trough intercellular contacts,[60] we decided to further study the effect of TAT-Cx43$_{266-283}$ on p120 catenin. First, we analyzed p120 catenin abundance and its subcellular location in G166 GSCs by immunocytochemistry. Our results revealed that p120 catenin was enriched in intercellular contact sites in control GSCs but not in TAT-Cx43$_{266-283}$--treated GSCs (Fig. 5F). In addition to its role in cell–cell junctions, p120 catenin plays a prominent role in the dynamics and regulation of lamellipodia,[61] a cytoskeletal projection involved in migration.[62] Indeed, control GSCs frequently presented p120-enriched lamellipodia, whereas these structures were less frequent and contained less p120 catenin in GSCs treated with TAT-Cx43$_{266-283}$ (Fig. 5F-H), indicating that TAT-Cx43$_{266-283}$ reduces p120 catenin abundance and decreases its critical location in cell-cell contacts and lamellipodia in G166 GSCs. Importantly, several of the proteins of the p120 catenin interaction network (SRC, CTNNB1, RHOA, PLEKHA7, CDH2, MLLT, protocadherin, cadherin and ZBTB family members, Supp. Fig. 5A) were identified in our samples, suggesting that this molecular pathway is in place in G166 GSCs.

Regarding the clinical relevance of p120 catenin, in samples from glioma patients, we explored the localization of *CTNND1* mRNA in different anatomic features of GBM, based on the data provided by the Ivy GAP database [63] (https://glioblastoma.alleninstitute.org) and found it is enriched in the microvascular proliferation area (Supp. Fig. 5B), a key pathologic feature of GBM not present in lower-grade glial tumors. Interestingly, *SRC* mRNA is also enriched in microvascular proliferation area (Supp. Fig. 5B), suggesting a correlation between *CTNND1* and *SRC*. Indeed, we found a significant correlation between *CTNND1* and *SRC* mRNAs in CGGA GBM patient dataset (Supp. Fig. 5C). In addition, *CTNND1* mRNA levels were elevated in glioma samples compared to healthy tissue but there were not significant differences between astrocytoma and GBM samples (Supp. Fig. 5D; however, lower mRNA levels of *CTNND1* correlated with better survival in glioma patients (Supp. Fig. 5E and reference [60]). In GBM patients, lower mRNA levels of *CTNND1* were associated with better survival, although the association was statistically significant only in 1 of the 3 datasets (Supp. Fig. 5E). We next analyzed the survival of GBM patients with lower levels of clinically relevant proteins decreased by TAT-Cx43$_{266-283}$ treatment, such as CLU, ITGA7, PXN and SDC1, and found a significant increase in survival (Fig. 5I). Importantly, when p120 catenin was included in this analysis, the survival rate was further improved (Fig. 5J), which suggests that the phenotypic changes promoted by TAT-Cx43$_{266-283}$, i.e., lower levels of CLU, ITGA7, PXN, SDC1 and p120, might strongly improve GBM patient survival.

To confirm the p120 results, we used different GSCs and an in vivo GBM model. We selected the syngeneic orthotopic GL261-GSC model in which TAT-Cx43$_{266-283}$ exerts an important anti-tumor effect enhancing the survival of GBM-bearing mice.[22] Murine GL261-GSCs were intracranially injected together with saline or TAT-Cx43$_{266-283}$ into the brains of immunocompetent mice and one week after tumor implantation, mice were intraperitoneally injected with TAT-Cx43$_{266-283}$ twice per week for 28 days and then the brains were processed, as illustrated in Fig. 6A. p120 was analyzed by immunohistochemistry in brain sections in both the core and the border of tumors of similar size and location (Fig. 6B and Supp. Fig. 6). Our results suggested a reduction in p120 expression promoted by TAT-Cx43$_{266-283}$ in murine GL261-GSCs located in the core of these tumors in vivo (Fig. 6C), although these results were not statistically significant (Fig. 6D). The location of p120 in some cells surrounding blood vessels (arrow in Fig. 6C as example) agrees with the enriched localization of *CTNND1* (p120) mRNA in the microvascular proliferation area found in GBM patients (Supp. Fig. 5B). Consistent with the role of p120 in GBM infiltration,[60] p120 was highly expressed by GBM cells located at the tumor border (Fig. 6E). Importantly, TAT-Cx43$_{266-283}$ treatment significantly reduced p120 expression in these infiltrative tumor cells located at the margin of the tumors (Fig. 6F). It should be highlighted that in contrast to the short-term in vitro studies, the in vivo analyses were performed in tumors, 28 days after tumor implantation and treatment. Therefore, these results suggest a durable effect of TAT-Cx43$_{266-283}$ on p120 expression, which is sustained over time.

Discussion

Our previous studies showed that TAT-Cx43$_{266-283}$ exerts antitumor effects in different preclinical models of GBM in vitro and in vivo.[20,22]

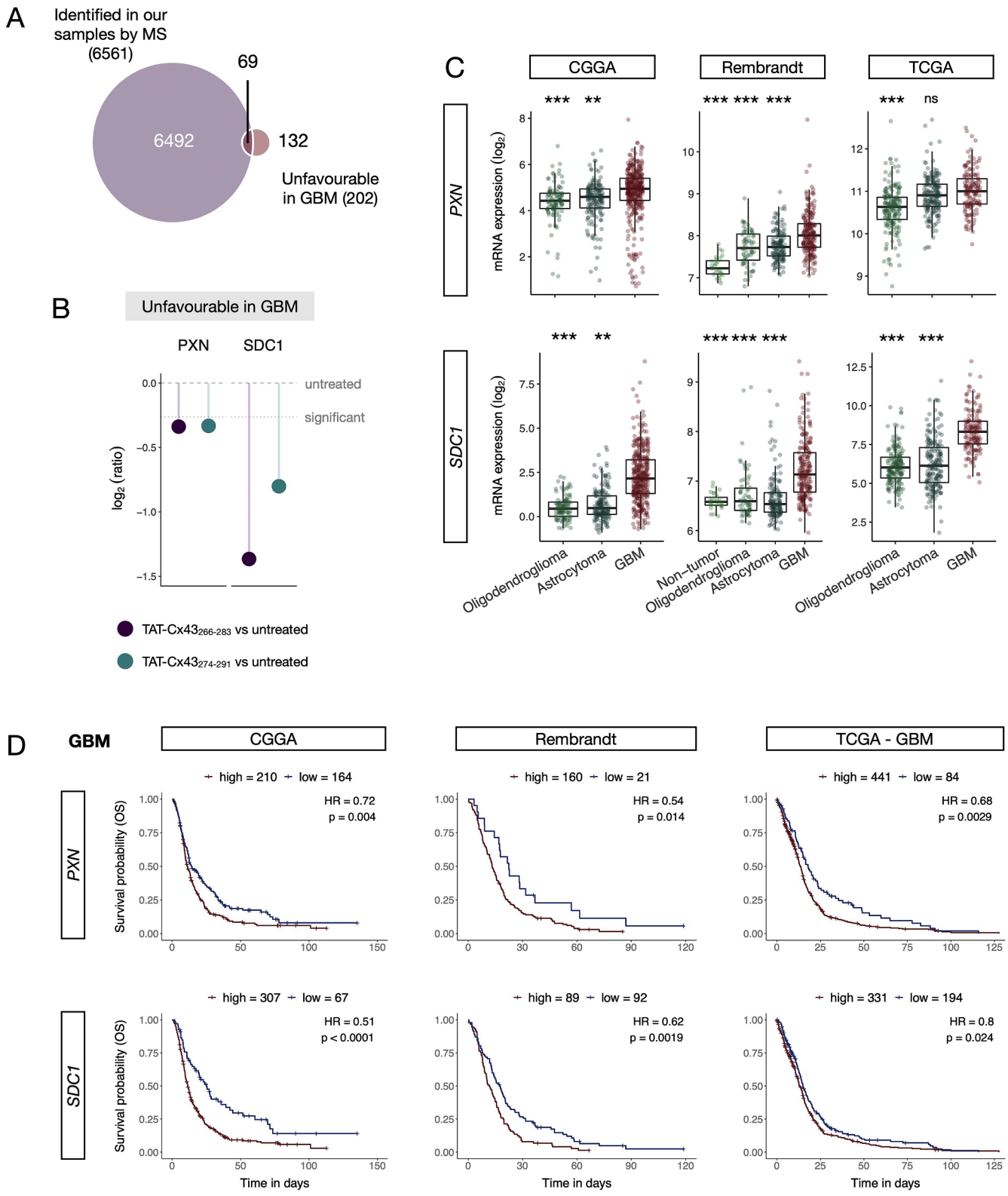

Fig. 4. TAT-Cx43$_{266-283}$ decreases the abundance of two proteins, paxillin and syndecan-1, that correlate with unfavorable prognosis in GBM. Proteins identified in our MS analysis were compared to genes correlated with unfavorable prognosis in GBM (the Pathology Atlas).

A. Venn diagram of proteins identified in our MS analysis and unfavorable genes in GBM.

B. The abundance of two proteins, paxillin (*PXN*) and syndecan-1 (*SDC1*), was significantly modified by TAT-Cx43$_{266-283}$ and TAT-Cx43$_{274-291}$ in our experiment.

C. mRNA levels of *PXN* and *SDC1* across glioma histology in 3 datasets shown as described in Fig. 3C. $^{**}P < 0.01$, $^{***}P < 0.001$, ns: not significant vs GBM (Tukey's Honest Significant Difference).

D. Kaplan-Meier curves of GBM patient survival associated with high or low mRNA levels of the indicated genes in 3 datasets. *P* values were obtained with the log-rank test.

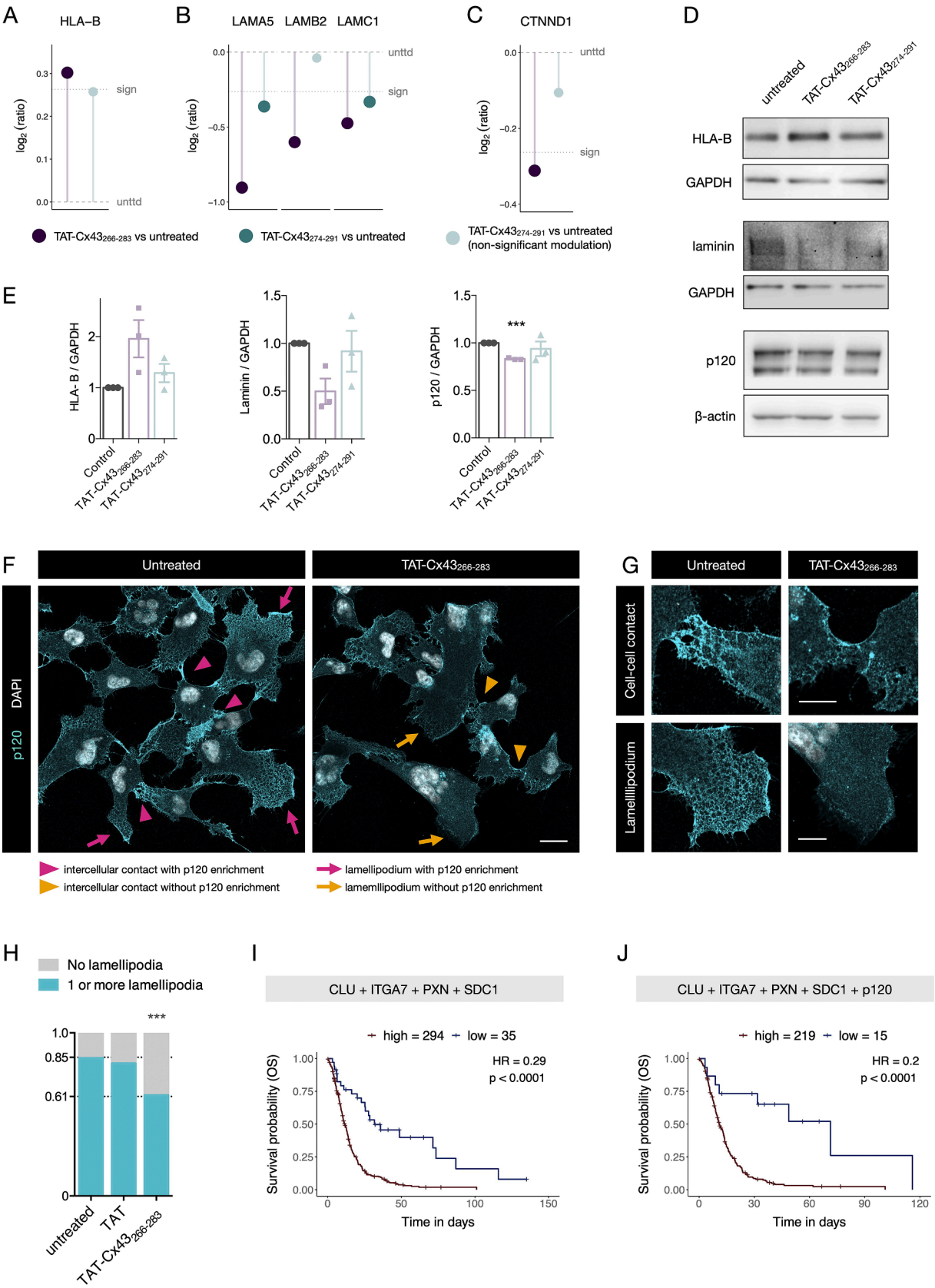

(caption on next page)

Fig. 5. TAT-Cx43$_{266-283}$ decreases the abundance of HLA-B (*HLA-B*), laminin 11 (*LAMA5, LAMB2, LAMC1*) and a classic c-Src substrate, p120 catenin (*CTNND1*).
A - C. MS-based relative protein abundance of HLA-B (A), laminin (B) and p120 catenin (C).
D. HLA-B, laminin and p120 catenin protein levels detected by western blotting (representative blots). GAPDH or β-actin are shown as loading controls. Triplicates and uncropped blots can be found in Supp. Fig. 4.
E. Quantifications of western blots.
F. G166 GSCs immunostained for p120 catenin. Pink and orange arrowheads indicate intercellular contacts with and without p120 catenin enrichment, respectively. Similarly, pink and orange arrows indicate lamellipodia with and without p120 catenin enrichment, respectively. Scale bar: 20 μm.
G. Zoomed-in images from (F) showing p120 catenin abundance in cell-cell contacts (upper panels) and lamellipodia (lower panels). Scale bar: 10 μm.
H. Quantification of lamellipodia per cell in G166 GSCs from three different experiments. G166 GSCs were immunostained for glucose transporter 1 (cell membrane marker) and lamellipodia were counted. ***$P < 0.001$ (Fisher's exact test).
I and J. Kaplan-Meier curves of GBM patient survival associated with high or low mRNA levels of the indicated gene signatures. *P* values were obtained with the log-rank test.

Although the molecular bases and the capability of TAT-Cx43$_{266-283}$ to inhibit Src are well known,[19] we cannot exclude that this peptide binds other intracellular targets, as multiple molecular partners converge in the 266-283 region of Cx43 [26]. In addition, Src is a node in a complex network of interacting proteins [64] and the effect of its inhibition may be unique for each inhibitor and for each context. Therefore, gaining a comprehensive view of the mechanism of action of TAT-Cx43$_{266-283}$ is essential to translate these promising preclinical results to a clinical setting. The main advantage of proteomics over other omics is that it provides information about protein levels, which, contrary to mRNA levels - which are not always predictive of protein levels [65] - ultimately regulate every cellular process.

As expected, cell metabolism [9] and cytoskeleton and membrane dynamics,[66] two Src-regulated pathways, are among the top biological pathways modulated by TAT-Cx43$_{266-283}$. Indeed, we previously showed that TAT-Cx43$_{266-283}$ impairs GSC metabolic plasticity and autophagy.[11,23] In line with this, this proteomic analysis unveiled new key metabolic regulators, such as mechanistic target of rapamycin (mTOR), fatty acid synthase (FAS), glutamine synthetase (GLUL) and isocitrate dehydrogenase 1 (IDH-1), which are down-regulated specifically by TAT-Cx43$_{266-283}$ and not by the non-antitumor peptide TAT-Cx43$_{274-291}$. All these metabolic regulators are involved in GBM growth, adaptation to lack of nutrients and resistance to therapy. Thus, mTOR, fatty acid synthase and glutamine synthetase play a pivotal role in GBM and are prominent targets for its therapy.[67-69] Furthermore, the activity of IDH-1 and glutamine synthetase increases resistance to radiotherapy,[70] which provides a rationale for the combination of radiotherapy with TAT-Cx43$_{266-283}$ for GBM therapy.

Regarding cytoskeleton and membrane dynamics, our previous study described how TAT-Cx43$_{266-283}$ impaired GBM invasion and migration in vitro and in vivo.[20,22] The present study uncovers prominent cytoskeletal proteins involved in cell adhesion, signal transduction and membrane dynamics, such as talin-1 (TLN1), catenin alpha1 (CTNNA1) and catenin delta1 or p120 (CTNND1), whose down-regulation may participate in the inhibition of invasion promoted by TAT-Cx43$_{266-283}$ previously reported.[20,22] Talin-1 adapts glioma cell mechanical properties to those of the surrounding microenvironment, contributing to glioma cell spreading and motility despite changes in extracellular matrix composition and stiffness.[71] Catenin alpha1 plays an important role in the cell adhesion process by connecting cadherins located on the plasma membrane to the actin filaments inside the cell. Although catenin alpha1 (which is up-regulated in GBM compared to low grade astrocytoma [72]) may inhibit glioma cell invasion by suppression of β-catenin transactivation,[73] this effect is disrupted by EGFR activation,[74] which is frequently overactivated in GBM. Therefore, it is difficult to predict the contribution of the down-regulation of catenin alpha1 promoted by TAT-Cx43$_{266-283}$ to the disruption of GSC invasion.

More evident is the contribution of catenin delta1 or p120 (CTNND1), necessary for GBM cells to migrate through the brain parenchyma in vivo.[60] First described as a Src substrate, whose phosphorylation correlated with malignant transformation,[75] p120 is a member of the Armadillo protein family, which function in adhesion between cells and signal transduction.[58] p120 binds to cadherins and regulates cytoskeletal reorganization through Rho GTPases [59] and is required for diffuse glioma infiltration, a function for which both the cadherin and Rho GTPase binding domains are necessary.[60] p120 has also been shown to be relevant for lamellipodial dynamics in cancer.[61] Importantly, our results showed that in addition to reducing p120 catenin levels in vitro and in vivo in human and murine GSCs, TAT-Cx43$_{266-283}$ treatment disrupted p120 specific location in cell-cell contacts and lamellipodia, suggesting a role in tumor cell migration. Indeed, TAT-Cx43$_{266-283}$ treatment reduced p120 expression in those infiltrative cells located at the tumor border in a murine in vivo GBM model. Therefore, our results suggest that the p120 reduction induced by TAT-Cx43$_{266-283}$ treatment might participate in the reduction of GSC invasiveness and the enhanced survival of GBM-bearing mice exerted by TAT-Cx43$_{266-283}$.[20,22].

Our results suggest a role of TAT-Cx43$_{266-283}$ not only in tumor cell properties but also in their interaction with the brain microenvironment by regulating the abundance of proteins related to the extracellular matrix, cell-cell interactions and the immune system response. As previously mentioned, the reduction in talin-1 levels may disrupt the adaptation to changes in extracellular matrix composition.[71] In addition, extracellular matrix signaling molecules, such as laminins (such as laminin 11, formed by the alpha-5 (LAMA5), beta-2 (LAMB2) and gamma-1 (LAMC1) subunits [33]) and their receptors, integrins (such as integrin-alpha-4 (ITGA4), integrin-alpha-7 (ITGA7), and integrin-beta-6 (ITGB6)), are down-regulated by TAT-Cx43$_{266-283}$ treatment in GSCs. Integrins also facilitate cell-cell and cell-extracellular matrix interactions and can trigger signaling transduction pathways, including Src related pathways.[34,35] Proteoglycans are also important components of the extracellular matrix within the tumor microenvironment. Among those affected by TAT-Cx43$_{266-283}$, only agrin (AGRN) is specifically down-regulated by this peptide and not by TAT-Cx43$_{274-291}$. Agrin plays an important role in the extracellular matrix and function of the blood brain barrier in GBM,[76] hence the modulation exerted by the Cx43 peptide might represent an opportunity to regulate its permeability to improve therapy penetration.

Intriguingly, Metascape analysis highlights "adaptative immune system" and "cytokine signaling in immune system" among the top pathways affected specifically by TAT-Cx43$_{266-283}$. Indeed, HLA-B (one of the 3 classic HLA class I proteins) was more abundant in GSCs after TAT-Cx43$_{266-283}$, but not after TAT-Cx43$_{274-291}$, treatment. Down-regulation of HLA aids GSCs in escaping immune surveillance through decreased antigen-presentation and T cell recruitment.[42-44] In addition, HLA participates in the regulation of cell stemness, and, therefore, a tumor-suppressing role for these proteins has been proposed.[77] These results suggest that TAT-Cx43$_{266-283}$ might affect the response of tumor associated immune cells and improve immunotherapy. Together, these proteomic results encourage further research to obtain a complete picture of the role of TAT-Cx43$_{266-283}$ on the immune system and the whole tumor microenvironment, which is critical for the development and support of GBM growth.[78]

Not all the proteins altered specifically by TAT-Cx43$_{266-283}$ are down-regulated; among the proteins whose levels are increased is HLA-B, described above, and other interesting proteins, such as Rab7A.

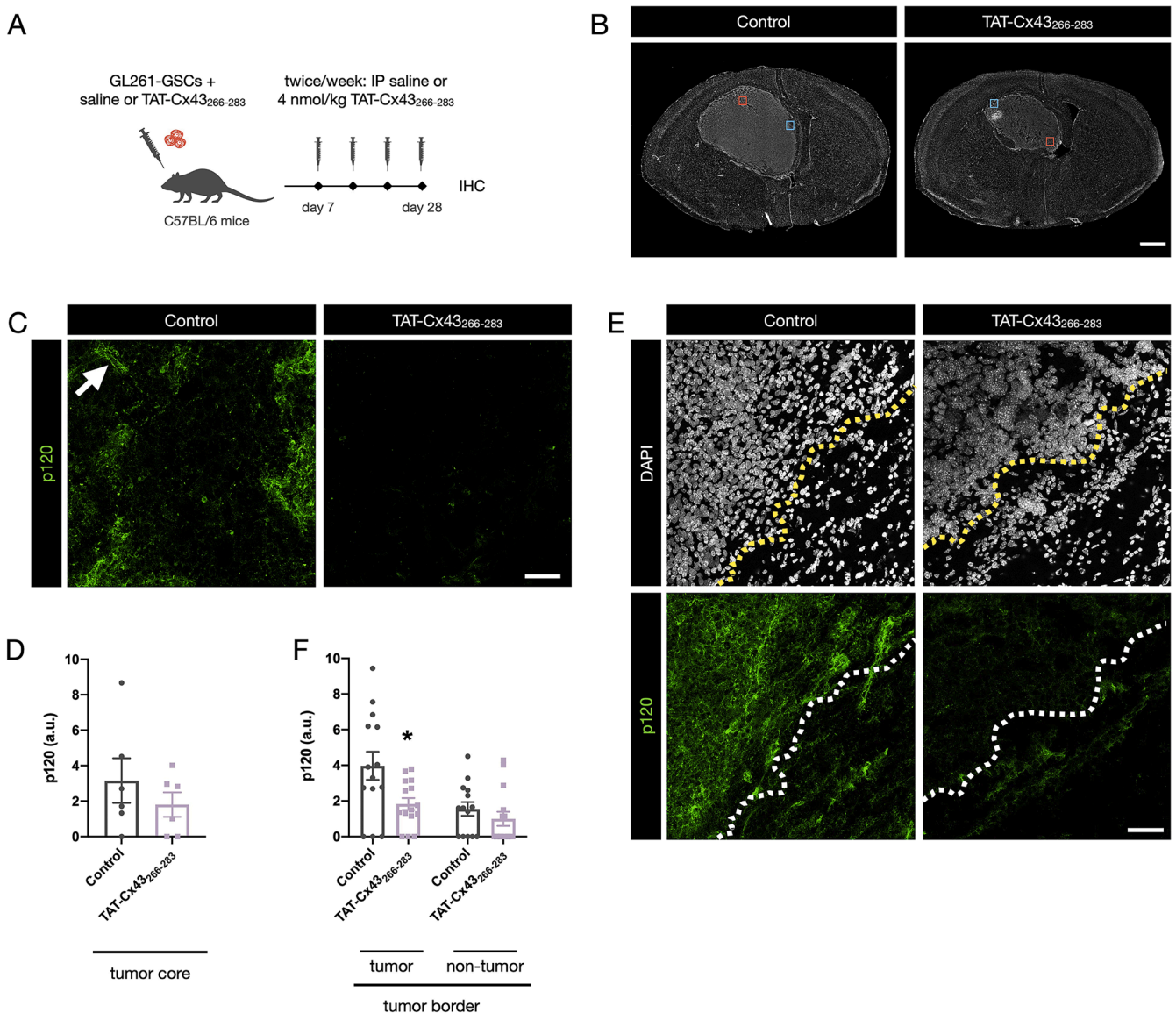

Fig. 6. TAT-Cx43$_{266-283}$ reduces p120 abundance in vivo in an immunocompetent GBM model.
A. GL261-GSCs together with saline or 100 μM TAT-Cx43$_{266-283}$ were intracranially injected in C57BL/6 mice. After 7 days, a twice per week IP injection of saline or 4 nmol/g of TAT-Cx43$_{266-283}$ was administered. 28 days post implantation, brains were processed for p120 immunohistochemistry (green) and DAPI nuclear staining (grey).
B. Representative images of DAPI staining in tumor brain sections from control and treated mice. Red squares: tumor core. Blue squares: tumor border. Bar: 1 mm. Triplicates can be found in Supp. Fig. 6.
C. p120 immunofluorescence in the core of the tumor of the sections shown in B (red squares). Arrowhead points to a blood vessel-like structure. Bar: 50 μm.
D. Quantification of p120 levels in the tumor core. Results are expressed in arbitrary units (a. u.) and are the mean±SEM from three independent experiments from which 2 fields were quantified.
E. p120 immunofluorescence in the border of the tumor (dashed line) of the sections shown in B (blue squares). Bar: 50 μm.
F. Quantification of p120 levels in the tumor area and non-tumor area of the tumor borders. Results are expressed in arbitrary units (a. u.) and are the mean±SEM from three independent experiments from which 4-6 fields were quantified. * $P < 0.05$ (Student's t-test).

Rab7A belongs to the Ras-like small-GTPase family and regulates endocytosis-mediated protein trafficking. Rab7A facilitates trafficking of receptor tyrosine kinases, including EGFR, from early endosome to late endosome and lysosome for their ultimate degradation.[79] Therefore, the up-regulation of Rab7a promoted by TAT-Cx43$_{266-283}$ might be taking part in the antitumor effect by increasing the proteolysis of pro-tumoral molecules.

Importantly, the unbiased analysis of the prognosis significance of those proteins whose abundance is increased by TAT-Cx43$_{266-283}$ showed that none of these modifications correlated with shorter survival in GBM patients. On the other hand, two proteins associated with worse prognosis, paxillin (PXN) and syndecan-1 (SDC1), were less abundant after treatment with TAT-Cx43$_{266-283}$ or TAT-Cx43$_{274-291}$. Paxilin, a well-known Src target found at focal adhesions, has been found to correlate with tumor progression and predict poor survival in GBM.[80] Syndecan-1, a transmembrane heparan sulphate proteoglycan, when knocked-down, can inhibit glioma cell proliferation via decreased phosphorylation of the Src/FAK axis,[81] so reduced syndecan-1 levels might contribute to TAT-Cx43$_{266-283}$'s inhibitory effect on Src. Similarly, Clusterin (*CLU*, also known as ApoJ) and integrin-alpha-7 (*ITGA7*) were less abundant specifically after treatment with TAT-Cx43$_{266-283}$ but not with TAT-Cx43$_{274-291}$ and are associated with shorter survival in all the

datasets tested. Clusterin (ApoJ) is a multifunctional protein involved in a wide range of biological processes, including lipid transport, membrane recycling, cell adhesion, programmed cell death, and complement cascade,[82] it is over-expressed in patient derived primary glioma cells compared to healthy brain tissue [83] and its secretion is part of the adaptive radioresistance response in GBM.[84] Interestingly, this response was found to rely on increased N-cadherin levels, a protein that is also down-regulated by TAT-Cx43$_{266-283}$ in GSCs.[21] As mentioned above, integrin-alpha-7 participates in the laminin-integrin signaling axis primarily by binding to laminin-1, 2 and 4.[85] In GBM, integrin-alpha-7 is a GSC marker and a promising therapeutic target.[86,87] In fact, knockdown of integrin-alpha-7 impairs growth and survival of GSCs and tumor formation in mouse models of glioma.[87] Although additional preclinical studies are required - stability, optimal dose and route of administration- and potential side effects cannot be excluded, our results strongly support that the changes in protein levels promoted by TAT-Cx43$_{266-283}$ may provide a clinical improvement for GBM patients.

Most of the new TAT-Cx43$_{266-283}$ modulated proteins identified in this study, such as p120,[57] mTOR,[88] fatty acid synthase,[89] glutamine synthetase,[89] laminins, integrins,[34] catenins,[75] clusterin,[90] Rab7A [91] and agrin [91] are somehow related to Src-signalling pathways, which supports the inhibition of Src in the antitumor mechanism of action of TAT-Cx43$_{266-283}$.[19-22] However, other proteins, such as HLA-B have not been so clearly described to be related to Src-signalling pathways, therefore, other TAT-Cx43$_{266-283}$ intracellular targets cannot be excluded.

Our proteomic study unveils new downstream effectors of TAT-Cx43$_{266-283}$, such as p120 catenin, for which we confirmed a decrease in abundance in vitro and in vivo, and a modification of subcellular localization in vitro. We also identified other putative effectors that deserve further research. Altogether, this study expands our knowledge about the mechanism of action of TAT-Cx43$_{266-283}$, providing a rationale for therapy combination and supporting its use in GBM clinical trials. These results may be extended and confirmed using phosphoproteomics or another type of omics to obtain orthogonal results. Importantly, we would like to highlight that this is an open study, which will provide much more information with the advancing knowledge of GBM biology.

Methods

Animals

Equal number of male and female C57BL/6 mice were obtained from the animal facility of the University of Salamanca. The animal procedures were approved by the ethics committee of the University of Salamanca and *Junta de Castilla y León* and were carried out in accordance with the European Community Council Directives (2010/63/UE), Spanish law (R.D. 53/2013 BOE 34/11370-420, 2013).

Cells

G166 human GSCs (RRID: CVCL_DG66) (IDH-wt) were obtained from BioRep and cultured as previously described [23] in RHB-A medium (Takara Bio Inc.) supplemented with 2% B27 (Life Technologies), 1% N2 (Life Technologies), 20 ng ml^{-1} EGF, and 20 ng ml^{-1} b-FGF (PeproTech) (complete medium) under adherent conditions, to maintain the GSC phenotype.[92] Culture plates were coated with 10 μg ml^{-1} laminin (Invitrogen, 23017-015) for 2 h before use. Cells were grown to confluence, dissociated using Accutase (Thermo Fisher), and then split to convenience. We routinely used cultures expanded for no more than 15 passages.

Mouse GL261-GSCs were cultured as spheres in stem cell medium supplemented with 1% B27, 0.5% N2, 10 ng ml^{-1} EGF and 20 ng ml^{-1} b-FGF, as previously described.[22] GL261-GSC spheres were dissociated using Accutase and subcultured as required every 10 to 14 days.

Treatments

Synthetic peptides (> 95% pure) were obtained from GenScript (Piscataway, NJ, USA) and used as previously described.[21] YGRKKRRQRRR was used as the TAT sequence, which enables the cell penetration of peptides.[93] The TAT-Cx43$_{266-283}$ sequence was TAT-AYFNGCSSPTAPLSPMSP (patent ID: ES2526109B1). The TAT-Cx43$_{274-291}$ sequence was TAT-PTAPLSPMSPPGYKLVTG.

Experimental design

G166 GSCs stemming from three different batches (different handlers, different freezer-storage periods and different number of freeze-thaw cycles) were considered biological replicates. Within each batch, three technical replicates were treated for each group: control (no treatment), TAT-Cx43$_{266-283}$ (peptide treatment) and TAT-Cx43$_{274-291}$ (negative control). After silver nitrate staining, one technical replicate from each group and each biological replicate was selected for subsequent MS analysis.

Sample collection and lyophilization

G166 GSCs were seeded in stem-cell, adherent conditions as previously described [23] in p12 multi-well dishes and treated when they reached 80% confluency. The cells were treated with TAT-Cx43$_{266-283}$ or TAT-Cx43$_{274-291}$ at 50 μM final concentration for 24 h. Then, they were quickly collected by enzymatic dissociation with Accutase, washed, pelleted and frozen at -80 °C. Subsequently, the cells were lyophilized by the Spanish DNA National Bank Carlos III Lyophilization Service in an Epsilon 2-4 LSCplus (Martin Christ) installation as follows: freezing step (3 h at -50 °C), first drying step (10 h at -20 °C and then 2 h at -10 °C, both at 0.38 mbar), final drying step (elevate temperature from -10 °C to 15 °C at 0.42 °C/min and 0.001 mbar, then elevate to 25 °C for up 4 h at 0.42 °C/min and 0.001 mbar). The temperature inside the samples did not surpass 20 °C at any given time during the process. Then, the samples were vacuum sealed and sent to the University of Geneva in dry ice.

Sample resuspension and protein quantification

Lyophilized cell pellets were carefully resuspended in 0.1% RapiGest (Waters) and 100 mM TEAB pH 8 (Sigma-Aldrich), sonicated (6 cycles of 20 s with breaks on ice) and centrifuged for 5 min at 4,000 x *g*. Then, the supernatant was recovered and the protein content was measured using the Bradford assay (Bio-Rad) in a microplate reader (FilterMax F3, Molecular Devices). Samples (lyophilized or resuspended) were stored at -80 °C.

SDS-PAGE gel electrophoresis for silver nitrate staining

Gels for SDS-PAGE (sodium dodecyl sulphate polyacrylamide gel electrophoresis) were prepared in a Hoefer Mighty Small II cast system (Hoefer). 12.5% acrylamide running gel and 4% acrylamide stacking gel solutions were prepared, containing: acrylamide, Tris-HCl 375 mM pH 8.8 for the running gel or Tris-HCl 125 mM pH 6.8 for the stacking gel, and water. To catalyze gel polymerization, TEMED (Tetra-methyl-ethylene-diamine) (final concentration for running gel: 0.1% and for stacking gel: 0.2%), and APS (final concentration for running gel: 0.02% and for stacking gel: 0.04%) were added at the final step to induce gel polymerization.

For each sample, the volume equivalent of 1 μg of sample was diluted in distilled H_2O and Laemmli buffer was added. The samples were then boiled at 95 °C for 5 min, centrifuged briefly and loaded in the SDS-PAGE gels. The electrophoresis was run at 70 mV for the first 45 min and then at 150 mV for 1 - 2 h. Then, the gels were incubated in fixation solution (30% ethanol, 7.5% acetic acid in water) for at least one hour at room temperature, or overnight at 4 °C, washed 3 times for 5 min in 10%

ethanol, incubated for 30 min in glutaraldehyde 1%, washed another 3 times for 5 min in 10% ethanol, and finally incubated for 30 min in the silver nitrate staining solution, which contained 0.2% silver nitrate, 0.28% ammonia and 0.2% NaOH in distilled H_2O. The gels were afterwards washed 4 times for 5 min in 10% ethanol and incubated for 1-5 min in development solution, containing 0.005% citric acid and 0.02% formaldehyde in distilled H_2O, and the development was stopped by incubation in 1% acetic acid for 30 min.

Sample preparation for MS

To avoid batch effects, all the samples were prepared together for MS. For each sample, the volume equivalent of 20 μg of protein was reduced using TCEP (tris(2-carboxyethyl)phosphine) (final concentration of 5 mM for 30 min at 37°C) (Sigma-Aldrich), alkylated using iodoacetamide (final concentration 15 mM for 60 min at RT in dark conditions) (Sigma-Aldrich), and digested overnight at 37 °C using trypsin (w/w ratio 1:50) (Pro-mega). The RapiGest surfactant was cleaved by incubating samples with trifluoroacetic acid (Sigma-Aldrich) (0.5% for 45 min at 37°C), and the pH was checked to be below 2 prior to incubation to ensure Rapigest cleavage. Samples were desalted on C18 reverse phase columns (Harvard Apparatus). Briefly, the columns were equilibrated with acetonitrile (ACN), then 50% ACN containing 0.1% formic acid (FA), and finally 5% ACN 0.1% FA twice. Then the columns were loaded with the samples, spun down, washed with 5% ACN FA 0.1% twice, and finally the samples were eluted with 50% ACN 0.1% FA. The peptides were dried under vacuum and subsequently resuspended in 5% ACN 0.1% FA and iRT peptides (Biognosys) (vol/vol 1:10) for MS. iRT peptides are 11 non-naturally occurring synthetic peptides that serve as internal standards and allow precise peptide normalization in DIA experiments. All solutions used in the preparation of the samples for MS were MS grade.

Data independent acquisition mass spectrometry (DIA-MS)

To avoid batch effects, the samples were injected sequentially on the same run. The equivalent of 2 μg of peptides was analyzed using liquid chromatography-electrospray ionization-MS/MS (LC-ESI-MS/MS) on an Orbitrap Fusion Lumos Tribrid mass spectrometer (Thermo Fisher Scientific) equipped with a Thermo EASY-nLC nLC1200 liquid chromatography system. Peptides were trapped on a 2 cm × 75 μm i.d. PepMap C18 precolumn packed with 3 μm particles and 100 Å pore size. Separation was performed using a 50 cm × 75 μm i.d. PepMap C18 column packed with 2 μm and 100 Å particles and heated at 50°C. Peptides were separated using a 160-min segmented gradient of 0.1% FA (solvent A) and 80% ACN 0.1% FA (solvent B), at a flow rate of 250 nl/min, following the published protocol.[94] Data-independent acquisition (DIA) was performed with MS1 full scan at a resolution of 60,000 (FWHM) followed by 30 DIA MS2 scan with variable windows. MS1 was performed in the Orbitrap with an AGC target of 1×10^6, a maximum injection time of 50 ms and a scan range from 400 to 1250 m/z. DIA MS2 was performed in the Orbitrap using higher-energy collisional dissociation (HCD) at 30%. Isolation windows (30) were variable with an AGC target of 2×10^6 and a maximum injection time of 54 ms.

DIA-MS data and proteins with significant changes in abundance

The raw DIA-MS data were matched to peptides using directDIA (version 2.0), a proprietary algorithm developed by Spectronaut™ (Biognosys), following the published protocol.[95] Briefly, directDIA is a library-free, spectrum-centric workflow that allows the analysis of DIA data without the need to generate a dedicated library, by searching the acquired DIA data against a protein database (in this case, the human proteome FASTA database) to identify the corresponding precursors (i.e., peptides) and calculate precursor intensities. Statistical analysis of protein differential expression was performed using mapDIA [96] based on precursor intensities exported from Spectronaut™. The parameters for mapDIA analysis were: experimental_design = replicate design, min correl = −1, min_obs = 3, min_pept_per_prot = 1, max_pept_per_prot = 15, min_DE = 0.01, max_DE = 0.99. Protein differential expression (i.e., change in abundance) was considered to change significatively when the FDR value (estimated Bayesian false discovery rate) [96] was < 0.05 and the absolute fold change ($|FC|$) was > 1.2 according to mapDIA results.

Data and pathway analysis

Correlation analysis, Venn diagram, PCA and volcano plots were performed in R.[97] Significant modifications in protein abundance were analyzed with MetaCore™ version 21.1 (Clarivate Analytics, Philadelphia, USA), Metascape [28] (https://metascape.org) and the String database [29] (https://string-db.org).

The human protein Atlas

The list of genes elevated or unfavorable in GBM according to the Pathology Atlas [50] analysis was downloaded from the glioma portal (https://www.proteinatlas.org/humanproteome/pathology/glioma, version 20.1). Their analysis was performed with TCGA transcriptomics data available from 153 patients; 54 female and 99 male, 30 were still alive and 123 patients deceased at the time of data collection.

Patient RNA levels and survival analysis

Patient data analysis was performed in the GlioVis data portal [51] (http://gliovis.bioinfo.cnio.es). mRNA levels plots and Kaplan-Meier curves were plotted in R [97] using data analyzed by GlioVis (downloaded May 2021). Three datasets were selected based on the number of GBM samples and the availability of histological information: the Chinese Glioma Genome Atlas [52] (CGGA), The Repository of Molecular Brain Neoplasia Data [53] (Rembrandt) and The Cancer Genome Atlas (TCGA GBM/LGG [55] and TGCA GBM [54] (HG-U133A), https://www.cancer.gov/tcga). For patient survival analysis, the mRNA cut-off for high or low level was determined by the 'optimal cut-off' section in GlioVis based on maximally selected rank statistics and applied to the data to generate the resulting survival plot and statistical analysis. Where this grouping variable was available, tumors from all groups were included in the analysis (i.e., primary, recurrent and secondary tumors). For the survival signature analyses (Fig. 5 J and K), patient data classified in high or low level groups by GlioVis were included in high or low level groups if they had high or low levels respectively for all the genes in the signature, and then survival analysis was performed as described above. The hazard ratio refers to the probability of dying by the next time point of a patient in the low levels group compared to a patient in the high levels group. The log-rank p value refers to the probability that the risk of death (hazard) is the same in both groups. The total number of patients of each glioma type can be found on Table S5.

Western blotting

Western blotting was performed as described previously.[23] Briefly, equal amounts of proteins across conditions were separated on NuPAGE Novex Bis-Tris 4-12% Midi gels (Life Technologies) at room temperature and constant voltage. Proteins were transferred to a nitrocellulose membrane (iBlot Gel Transfer Stacks Nitrocellulose) using an iBlot dry blotting system (Life Technologies). After blocking, the membranes were incubated overnight at 4°C with primary anti- bodies: rabbit polyclonal antibody against HLA-B (1:2,500; Abcam ab193415), rabbit polyclonal antibody against laminin (1:1,000; Sigma L9393; RRID: AB_477163), mouse monoclonal antibody against p120 (1:200; BD Transduction 610134; RRID:AB_397537), mouse monoclonal antibody against glyceraldehyde phosphate dehydrogenase (GAPDH; 1:5,000; Thermo Fisher Scientific AM4300; RRID: AB_437392) and rabbit

polyclonal antibody against glucose transporter 1 (1:500; Abcam ab652; RRID:AB_305540). After washing, the membranes were incubated with peroxidase-conjugated anti-rabbit IgG or anti-mouse IgG antibodies (1:5,000; Jackson ImmunoResearch) and developed with a chemiluminescent substrate (Western Blotting Luminol Reagent; Santa Cruz Biotechnology) in a MicroChemi imaging system (Bioimaging Systems). Original and replicate blots are shown in the Supplementary Figures. GAPDH protein levels in the same lanes were used as loading controls.

In vivo GBM model

Intracranial implantation of mouse GL261-GLSCs was carried out as described.[22] Briefly, a unilateral intracerebral injection of 1 μl of physiological saline containing 5,000 cells was injected in the right cortex at the following coordinates: 1 mm rostral to lambda, 1 mm lateral, and 2 mm deep. In treated animals, 100 μM TAT-$Cx43_{266-283}$ was co-injected with cells. After 7 days, saline or 4 nmol/g TAT-$Cx43_{266-283}$ were intraperitoneally injected twice per week. After 28 days, mice were anesthetized with pentobarbital (120 mg/kg, 0.2 ml) and transcardially perfused with 15 ml of physiological saline. Brains were then removed, fresh-frozen in liquid nitrogen, and kept at −80°C until used.

Immunofluorescence

Immunofluorescence was performed as described previously.[23] GSCs were fixed in methanol for 10 min at -20°C. The cells were then rinsed in PBS and incubated for 1 h in blocking solution (PBS containing 10% FCS, 0.1 M lysine, and 0.02% azide) with anti-mouse IgG (Jackson ImmunoResearch Ref. 115-007-003). The samples were incubated overnight at 4°C with mouse monoclonal antibody against p120 (1:100; BD Transduction 610134; RRID:AB_397537) prepared in blocking/permeabilisation solution (with 0.1% Triton X-100). After repeated washes, they were incubated with anti-mouse IgG Alexa Fluor 488-conjugated secondary antibody (1:1,000; Life Technologies) prepared in blocking/permeabilisation solution. Finally, nuclear DNA was stained with 1 μg/ml 4'-6- diamidino-2-phenylindole (DAPI) for 1 min. Cells were mounted using SlowFade Light antifade (Life Technologies) and imaged on an inverted Zeiss Axio Observer Z1 microscope for Live-Cell Imaging (Carl Zeiss Microscopy) coupled to an AxioCam MRm camera and Zeiss Apotome (optical sectioning structured illumination microscopy; https://www.zeiss.com/microscopy/int/solutions/reference/all-tutorials/optical-sectioning/apotome-operation.html). The images in Fig. 5 G and H are representative of three biological replicates.

For in vivo studies, 20-μm-thick coronal sections were processed for immunostaining. After fixing with 4% PFA for 25 min, brain sections were blocked for 2h in PBS containing 10% NGS, 5% BSA, 0.1% Tween, and 0.02% azide and incubated overnight at 4°C with mouse monoclonal antibody against p120 (1:100; BD Transduction 610134; RRID: AB_397537) prepared in the same solution (with 0.1% Tween). After repeating washing in PBS with 0.1% Tween, sections were incubated at 4°C overnight with a goat anti-mouse IgG Alexa Fluor A488-conjugated secondary antibody (1:500, Invitrogen, ref: #A-11029) prepared in PBS containing 10% NGS, 5% BSA, 0.1% Tween, and 0.02% azide. Nuclear DNA was stained with DAPI for 5 min and sections mounted using SlowFade Light antifade (Life Technologies). Mosaic images of the sections were acquired using a Leica Stellaris 8 confocal microscope, selecting only 1 plane of the z axis using a 10X objective (whole section images) or 5 planes of the z axis using a 63X objective (zoom-in images) (the maximum Z projection is shown in the figures).

Statistical analysis

Please refer to each Methods section for statistical analysis performed for high-throughput protein, RNA and patient data analyses. For comparison between two groups, data were analyzed by two-tailed Student's t-test. When more than two groups were compared, data were analysed by one-way ANOVA, and confidence intervals (95%) and significance were corrected for multiple comparisons with the Tukey test. In Fig. 5 I, proportions were compared with Fisher's exact test.

Data availability

The mass spectrometry proteomics data are available in the ProteomeXchange Consortium via the PRIDE [98] partner repository (http://www.ebi.ac.uk/pride) with the dataset identifier PXD045883. Project Name: DIA-MS proteomics of untreated and TAT-Cx43266-283-treated G166 GSCs. Reviewer account details: Username: reviewer_pxd045883@ebi.ac.uk and Password: avbslUzA. Table S1 and S2 contain proteins with a significant change in abundance versus untreated (FDR < 0.05, $|FC| > 1.2$) after TAT-$Cx43_{266-283}$ and TAT-$Cx43_{274-291}$ treatment, respectively, in G166 GSCs. Table S3 contains genes whose mRNA level was found to be elevated in GBM by the Pathology Atlas. Table S4 contains genes whose mRNA level was found to be correlated with unfavorable prognosis in GBM (the Pathology Atlas). Table S5 contains the number of patients for the survival analysis. Table S6 and S7 contain the results of the pathway analysis from Metascape for TAT-$Cx43_{266-283}$ and TAT-$Cx43_{274-291}$ treated GSCs, respectively.

CRediT authorship contribution statement

Sara G. Pelaz: Writing – review & editing, Writing – original draft, Methodology, Investigation, Formal analysis, Data curation, Conceptualization. **Raquel Flores-Hernández:** Writing – review & editing, Validation, Methodology, Investigation, Formal analysis. **Tatjana Vujic:** Writing – review & editing, Methodology, Investigation, Formal analysis, Data curation. **Domitille Schvartz:** Writing – review & editing, Methodology, Investigation, Formal analysis, Data curation, Conceptualization. **Andrea Álvarez-Vázquez:** Writing – review & editing, Validation, Methodology, Investigation. **Yuxin Ding:** Writing – review & editing, Validation, Methodology, Investigation. **Laura García-Vicente:** Writing – review & editing, Validation, Methodology, Investigation. **Aitana Belloso:** Writing – review & editing, Validation, Methodology, Investigation. **Rocío Talaverón:** Writing – review & editing, Validation, Methodology, Investigation. **Jean-Charles Sánchez:** Writing – review & editing, Supervision, Resources, Conceptualization. **Arantxa Tabernero:** Writing – review & editing, Writing – original draft, Supervision, Resources, Funding acquisition, Conceptualization.

Acknowledgements

This research was funded by Junta de Castilla y León, FEDER SA125P20 and the grants FEDER PID2021-128549OB-I00 funded by MCIN/AEI/ 10.13039/501100011033 and "ERDF A way of making Europe," and PDC2022-133652-I00 funded by MCIN/AEI/ 10.13039/501100011033 and "European Union NextGenerationEU/PRTR". Sara G. Pelaz was supported by Junta de Castilla y León (Orden EDU 529/2017) and an EMBO Short-Term Fellowship (#8674). R. Flores-Hernández and A. Álvarez-Vázquez were PhD fellowship recipients and Yuxin Ding "Programa Investigo" fellowship recipient from the Junta de Castilla y León, Servicio Público de Empleo Estatal and the European Social Fund, NextGenerationEU. L. García-Vicente was supported by the Spanish Ministerio de Universidades. We thank T. del Rey for technical assistance, TBI lab and proteomics core UNIGE and the Spanish DNA National Bank Carlos III Lyophilization Service. We would also like to thank Alexandre Hainard, Carla Pasquarello and Patrizia Arboit from the Proteomics Core Facility, Faculty of Medicine, University of Geneva, Switzerland for their kind help and advice for the proteomic analyses by mass spectrometry.

Authors declare that the only potential conflict of interest is that A.T. is an inventor on the patent (ID: ES2526109B1) from the University of Salamanca and that no sources of editorial support were used for

preparation of the manuscript. All authors read the journal's authorship agreement, revised the article for important intellectual content and approved the final version for publication.

Supplementary materials

Supplementary material associated with this article can be found, in the online version, at doi:10.1016/j.trsl.2024.06.001.

References

1. Louis DN, Perry A, Wesseling P, et al. The 2021 WHO classification of tumors of the central nervous system: a summary. *Neuro Oncol*. 2021;23(8):1231–1251.
2. Wen PY, Weller M, Lee EQ, et al. Glioblastoma in adults: a Society for Neuro-Oncology (SNO) and European Society of Neuro-Oncology (EANO) consensus review on current management and future directions. *Neuro Oncol*. 2020;22(8):1073–1113.
3. Stupp R, Taillibert S, Kanner A, et al. Effect of tumor-treating fields plus maintenance temozolomide vs maintenance temozolomide alone on survival in patients with glioblastoma: a randomized clinical trial. *JAMA*. 2017;318(23):2306–2316.
4. Chen J, Li Y, Yu TS, et al. A restricted cell population propagates glioblastoma growth after chemotherapy. *Nature*. 2012;488(7412):522–526.
5. Bao S, Wu Q, McLendon RE, et al. Glioma stem cells promote radioresistance by preferential activation of the DNA damage response. *Nature*. 2006;444(7120):756–760.
6. Han X, Zhang W, Yang X, et al. The role of Src family kinases in growth and migration of glioma stem cells. *Int J Oncol*. 2014;45(1):302–310.
7. Weissenberger J, Steinbach JP, Malin G, Spada S, Rulicke T, Aguzzi A. Development and malignant progression of astrocytomas in GFAP-v-src transgenic mice. *Oncogene*. 1997;14(17):2005–2013.
8. Martin GS. The hunting of the Src. *Nat Rev Mol Cell Biol*. 2001;2(6):467–475.
9. Pelaz SG, Tabernero A. Src: coordinating metabolism in cancer. *Oncogene*. 2022;41(45):4917–4928.
10. Du J, Bernasconi P, Clauser KR, et al. Bead-based profiling of tyrosine kinase phosphorylation identifies SRC as a potential target for glioblastoma therapy. *Nat Biotechnol*. 2009;27(1):77–83.
11. Pelaz SG, Ollauri-Ibáñez C, Lillo C, Tabernero A. Impairment of autophagic flux participates in the antitumor effects of TAT-Cx43. *Cancers*. 2021;13(17).
12. Ahluwalia MS, de Groot J, Liu WM, Gladson CL. Targeting SRC in glioblastoma tumors and brain metastases: rationale and preclinical studies. *Cancer Lett*. 2010;298(2):139–149.
13. de Groot J, Milano V. Improving the prognosis for patients with glioblastoma: the rationale for targeting Src. *J Neurooncol*. 2009;95(2):151–163.
14. Lassman AB, Pugh SL, Gilbert MR, et al. Phase 2 trial of dasatinib in target-selected patients with recurrent glioblastoma (RTOG 0627). *Neuro Oncol*. 2015;17(7):992–998.
15. Galanis E, Anderson SK, Twohy EL, et al. A phase 1 and randomized, placebo-controlled phase 2 trial of bevacizumab plus dasatinib in patients with recurrent glioblastoma: Alliance/North Central Cancer Treatment Group N0872. *Cancer*. 2019;125(21):3790–3800.
16. Higuchi M, Ishiyama K, Maruoka M, Kanamori R, Takaori-Kondo A, Watanabe N. Paradoxical activation of c-Src as a drug-resistant mechanism. *Cell Rep*. 2021;34(12),108876.
17. Martellucci S, Clementi L, Sabetta S, Mattei V, Botta L, Angelucci A. Src family kinases as therapeutic targets in advanced solid tumors: what we have learned so far. *Cancers*. 2020;12(6).
18. Herrero-Gonzalez S, Gangoso E, Giaume C, Naus CC, Medina JM, Tabernero A. Connexin43 inhibits the oncogenic activity of c-Src in C6 glioma cells. *Oncogene*. 2010;29(42):5712–5723.
19. Gonzalez-Sanchez A, Jaraiz-Rodriguez M, Dominguez-Prieto M, Herrero-Gonzalez S, Medina JM, Tabernero A. Connexin43 recruits PTEN and Csk to inhibit c-Src activity in glioma cells and astrocytes. *Oncotarget*. 2016;7(31):49819–49833.
20. Jaraíz-Rodríguez M, Tabernero MD, González-Tablas M, et al. A short region of Connexin43 reduces human glioma stem cell migration, invasion, and survival through Src, PTEN, and FAK. *Stem Cell Reports*. 2017;9(2):451–463.
21. Gangoso E, Thirant C, Chneiweiss H, Medina JM, Tabernero A. A cell-penetrating peptide based on the interaction between c-Src and connexin43 reverses glioma stem cell phenotype. *Cell Death Dis*. 2014;5.
22. Jaraíz-Rodríguez M, Talaverón R, García-Vicente L, et al. Connexin43 peptide, TAT-Cx43266-283, selectively targets glioma cells, impairs malignant growth, and enhances survival in mouse models in vivo. *Neuro Oncol*. 2020;22(4):493–504.
23. Pelaz SG, Jaraíz-Rodríguez M, Álvarez-Vázquez A, et al. Targeting metabolic plasticity in glioma stem cells in vitro and in vivo through specific inhibition of c-Src by TAT-Cx43. *EBioMedicine*. 2020;62, 103134.
24. Ludwig C, Gillet L, Rosenberger G, Amon S, Collins BC, Aebersold R. Data-independent acquisition-based SWATH-MS for quantitative proteomics: a tutorial. *Mol Syst Biol*. 2018;14(8):e8126.
25. Krasny L, Huang PH. Data-independent acquisition mass spectrometry (DIA-MS) for proteomic applications in oncology. *Mol Omics*. 2021;17(1):29–42.
26. Tabernero A, Gangoso E, Jaraíz-Rodríguez M, Medina JM. The role of connexin43-Src interaction in astrocytomas: a molecular puzzle. *Neuroscience*. 2016;323:183–194.
27. Spagnol G, Kieken F, Kopanic JL, et al. Structural studies of the Nedd4 WW domains and their selectivity for the Connexin43 (Cx43) carboxyl terminus. *J Biol Chem*. 2016;291(14):7637–7650.
28. Zhou Y, Zhou B, Pache L, et al. Metascape provides a biologist-oriented resource for the analysis of systems-level datasets. *Nat Commun*. 2019;10(1):1523.
29. Szklarczyk D, Gable AL, Nastou KC, et al. The STRING database in 2021: customizable protein-protein networks, and functional characterization of user-uploaded gene/measurement sets. *Nucleic Acids Res*. 2021;49(D1):D605–D612.
30. Tsukita S, Yonemura S, Tsukita S. ERM proteins: head-to-tail regulation of actin-plasma membrane interaction. *Trends Biochem Sci*. 1997;22(2):53–58.
31. Solinet S, Mahmud K, Stewman SF, et al. The actin-binding ERM protein Moesin binds to and stabilizes microtubules at the cell cortex. *J Cell Biol*. 2013;202(2):251–260.
32. Goldman RD, Khuon S, Chou YH, Opal P, Steinert PM. The function of intermediate filaments in cell shape and cytoskeletal integrity. *J Cell Biol*. 1996;134(4):971–983.
33. Miner JH, Patton BL. Laminin-11. *Int J Biochem Cell Biol*. 1999;31(8):811–816.
34. Playford MP, Schaller MD. The interplay between Src and integrins in normal and tumor biology. *Oncogene*. 2004;23(48):7928–7946.
35. Ellert-Miklaszewska A, Poleszak K, Pasierbinska M, Kaminska B. Integrin signaling in glioma pathogenesis: from biology to therapy. *Int J Mol Sci*. 2020;21(3):888.
36. Kikkawa Y, Sanzen N, Fujiwara H, Sonnenberg A, Sekiguchi K. Integrin binding specificity of laminin-10/11: laminin-10/11 are recognized by alpha 3 beta 1, alpha 6 beta 1 and alpha 6 beta 4 integrins. *J Cell Sci*. 2000;113(5):869–876.
37. Bishop JR, Schuksz M, Esko JD. Heparan sulphate proteoglycans fine-tune mammalian physiology. *Nature*. 2007;446(7139):1030–1037.
38. Fuster MM, Esko JD. The sweet and sour of cancer: glycans as novel therapeutic targets. *Nat Rev Cancer*. 2005;5(7):526–542.
39. Kakkar AK, Levine MN, Kadziola Z, et al. Low molecular weight heparin, therapy with dalteparin, and survival in advanced cancer: the Fragmin Advanced Malignancy Outcome Study (FAMOUS). *J Clin Oncol*. 2004;22(10):1944–1948.
40. Nduom EK, Weller M, Heimberger AB. Immunosuppressive mechanisms in glioblastoma. *Neuro Oncol*. 2015;17(suppl_7):vii9–vii14.
41. Weenink B, French PJ, Sillevis Smitt PAE, Debets R, Geurts M. Immunotherapy in glioblastoma: current shortcomings and future perspectives. *Cancers*. 2020;12(3):751.
42. Di Tomaso T, Mazzoleni S, Wang E, et al. Immunobiological characterization of cancer stem cells isolated from glioblastoma patients. *Clin Cancer Res*. 2010;16(3):800.
43. Morrison BJ, Steel JC, Morris JC. Reduction of MHC-I expression limits T-lymphocyte-mediated killing of Cancer-initiating cells. *BMC Cancer*. 2018;18(1):469.
44. Yang W, Li Y, Gao R, Xiu Z, Sun T. MHC class I dysfunction of glioma stem cells escapes from CTL-mediated immune response via activation of Wnt/β-catenin signaling pathway. *Oncogene*. 2020;39(5):1098–1111.
45. Minata M, Audia A, Shi J, et al. Phenotypic plasticity of invasive edge glioma stem-like cells in response to ionizing radiation. *Cell Rep*. 2019;26(7):1893–1905.e1897.
46. Shiraki Y, Mii S, Enomoto A, et al. Significance of perivascular tumour cells defined by CD109 expression in progression of glioma. *J Pathol*. 2017;243(4):468–480.
47. Li C, Cho HJ, Yamashita D, et al. Tumor edge-to-core transition promotes malignancy in primary-to-recurrent glioblastoma progression in a PLAGL1/CD109-mediated mechanism. *Neurooncol Adv*. 2020;2(1).
48. Bastola S, Pavlyukov MS, Yamashita D, et al. Glioma-initiating cells at tumor edge gain signals from tumor core cells to promote their malignancy. *Nat Commun*. 2020;11(1):4660.
49. Filppu P, Tanjore Ramanathan J, Granberg KJ, et al. CD109-GP130 interaction drives glioblastoma stem cell plasticity and chemoresistance through STAT3 activity. *JCI Insight*. 2021;6(9).
50. Uhlen M, Zhang C, Lee S, et al. A pathology atlas of the human cancer transcriptome. *Science*. 2017;357(6352):eaan2507.
51. Bowman RL, Wang Q, Carro A, Verhaak RG, Squatrito M. GlioVis data portal for visualization and analysis of brain tumor expression datasets. *Neuro Oncol*. 2017;19(1):139–141.
52. Zhao Z, Meng F, Wang W, Wang Z, Zhang C, Jiang T. Comprehensive RNA-seq transcriptomic profiling in the malignant progression of gliomas. *Sci Data*. 2017;4,170024.
53. Madhavan S, Zenklusen JC, Kotliarov Y, Sahni H, Fine HA, Buetow K. Rembrandt: helping personalized medicine become a reality through integrative translational research. *Mol Cancer Res*. 2009;7(2):157–167.
54. Brennan Cameron W, Verhaak Roel GW, McKenna A, et al. The somatic genomic landscape of glioblastoma. *Cell*. 2013;155(2):462–477.
55. Ceccarelli M, Barthel Floris P, Malta Tathiane M, et al. Molecular profiling reveals biologically discrete subsets and pathways of progression in diffuse glioma. *Cell*. 2016;164(3):550–563.
56. Aumailley M. The laminin family. *Cell Adh Migr*. 2013;7(1):48–55.
57. Reynolds AB, Herbert L, Cleveland JL, Berg ST, Gaut JR. p120, a novel substrate of protein tyrosine kinase receptors and of p60v-src, is related to cadherin-binding factors beta-catenin, plakoglobin and armadillo. *Oncogene*. 1992;7(12):2439–2445.
58. Alemà S, Salvatore AM. p120 catenin and phosphorylation: Mechanisms and traits of an unresolved issue. *Biochimica et Biophysica Acta (BBA) - Mol Cell Res*. 2007;1773(1):47–58.
59. Kourtidis A, Ngok SP, Anastasiadis PZ, van Roy F. *Chapter eighteen - p120 Catenin: an essential regulator of cadherin stability, adhesion-induced signaling, and cancer progression*. In: *Progress in Molecular Biology and Translational Science*. 116. Academic Press; 2013:409–432.
60. Gritsenko PG, Atlasy N, Dieteren CEJ, et al. p120-catenin-dependent collective brain infiltration by glioma cell networks. *Nat Cell Biol*. 2020;22(1):97–107.

61. Boguslavsky S, Grosheva I, Landau E, et al. p120 catenin regulates lamellipodial dynamics and cell adhesion in cooperation with cortactin. *Proc Natl Acad Sci USA*. 2007;104(26):10882–10887.
62. Yamaguchi H, Condeelis J. Regulation of the actin cytoskeleton in cancer cell migration and invasion. *Biochim Biophys Acta*. 2007;1773(5):642–652.
63. Puchalski RB, Shah N, Miller J, et al. An anatomic transcriptional atlas of human glioblastoma. *Science*. 2018;360(6389):660–663.
64. Parsons SJ, Parsons JT. Src family kinases, key regulators of signal transduction. *Oncogene*. 2004;23(48):7906–7909.
65. Liu Y, Beyer A, Aebersold R. On the dependency of cellular protein levels on mRNA abundance. *Cell*. 2016;165(3):535–550.
66. Angers-Loustau A, Hering R, Werbowetski TE, Kaplan DR, Del Maestro RF. SRC regulates actin dynamics and invasion of malignant glial cells in three dimensions. *Mol Cancer Res*. 2004;2(11):595–605.
67. Mecca C, Giambanco I, Donato R, Arcuri C. Targeting mTOR in glioblastoma: rationale and preclinical/clinical evidence. *Dis Markers*. 2018;2018, 9230479.
68. Zhao W, Kridel S, Thorburn A, et al. Fatty acid synthase: a novel target for antiglioma therapy. *Br J Cancer*. 2006;95(7):869–878.
69. Tardito S, Oudin A, Ahmed SU, et al. Glutamine synthetase activity fuels nucleotide biosynthesis and supports growth of glutamine-restricted glioblastoma. *Nat Cell Biol*. 2015;17(12):1556–1568.
70. Zhou W, Yao Y, Scott AJ, et al. Purine metabolism regulates DNA repair and therapy resistance in glioblastoma. *Nat Commun*. 2020;11(1):3811.
71. Sen S, Ng WP, Kumar S. Contributions of talin-1 to glioma cell-matrix tensional homeostasis. *J R Soc Interface*. 2012;9(71):1311–1317.
72. Shinoura N, Paradies NE, Warnick RE, et al. Expression of N-cadherin and alpha-catenin in astrocytomas and glioblastomas. *Br J Cancer*. 1995;72(3):627–633.
73. Ji H, Wang J, Fang B, Fang X, Lu Z. α-Catenin inhibits glioma cell migration, invasion, and proliferation by suppression of β-catenin transactivation. *J Neurooncol*. 2011;103(3):445–451.
74. Ji H, Wang J, Nika H, et al. EGF-induced ERK activation promotes CK2-mediated disassociation of alpha-Catenin from beta-Catenin and transactivation of beta-Catenin. *Mol Cell*. 2009;36(4):547–559.
75. Reynolds AB. p120-catenin: past and present. *Biochim Biophys Acta*. 2007;1773(1):2–7.
76. Rascher G, Fischmann A, Kröger S, Duffner F, Grote EH, Wolburg H. Extracellular matrix and the blood-brain barrier in glioblastoma multiforme: spatial segregation of tenascin and agrin. *Acta Neuropathol*. 2002;104(1):85–91.
77. Pujadas E, Cordon-Cardo C. The human leukocyte antigen as a candidate tumor suppressor. *Cancer Cell*. 2021;39(5):586–589.
78. Quail DF, Joyce JA. The microenvironmental landscape of brain tumors. *Cancer Cell*. 2017;31(3):326–341.
79. Ceresa BP, Bahr SJ. rab7 activity affects epidermal growth factor:epidermal growth factor receptor degradation by regulating endocytic trafficking from the late endosome. *J Biol Chem*. 2006;281(2):1099–1106.
80. Sun L-H, Yang F-Q, Zhang C-B, et al. Overexpression of paxillin correlates with tumor progression and predicts poor survival in glioblastoma. *CNS Neurosci Ther*. 2017;23(1):69–75.
81. Shi S, Zhong D, Xiao Y, et al. Syndecan-1 knockdown inhibits glioma cell proliferation and invasion by deregulating a c-src/FAK-associated signaling pathway. *Oncotarget*. 2017;8(25):40922–40934.
82. Koltai T. Clusterin: a key player in cancer chemoresistance and its inhibition. *OncoTargets Ther*. 2014;7:447–456.
83. Autelitano F, Loyaux D, Roudières S, et al. Identification of novel tumor-associated cell surface sialoglycoproteins in human glioblastoma tumors using quantitative proteomics. *PLoS One*. 2014;9(10), e110316.
84. Osuka S, Zhu D, Zhang Z, et al. N-cadherin upregulation mediates adaptive radioresistance in glioblastoma. *J Clin Invest*. 2021;131(6).
85. Cohn RD, Mayer U, Saher G, et al. Secondary reduction of α7B integrin in laminin α2 deficient congenital muscular dystrophy supports an additional transmembrane link in skeletal muscle. *J Neurol Sci*. 1999;163(2):140–152.
86. Carrasco-Garcia E, Auzmendi-Iriarte J, Matheu A. Integrin α7: a novel promising target in glioblastoma stem cells. *Stem Cell Investig*. 2018;5:2. -2.
87. Haas TL, Sciuto MR, Brunetto L, et al. Integrin α7 is a functional marker and potential therapeutic target in glioblastoma. *Cell Stem Cell*. 2017;21(1):35–50.e39.
88. Chi Y, Gao K, Li K, et al. Purinergic control of AMPK activation by ATP released through connexin 43 hemichannels - pivotal roles in hemichannel-mediated cell injury. *J Cell Sci*. 2014;127(Pt 7):1487–1499.
89. Bastie CC, Zong H, Xu J, et al. Integrative metabolic regulation of peripheral tissue fatty acid oxidation by the SRC kinase family member Fyn. *Cell Metab*. 2007;5(5):371–381.
90. Herault Y, Chatelain G, Brun G, Michel D. V-src-induced-transcription of the avian clusterin gene. *Nucleic Acids Res*. 1992;20(23):6377–6383.
91. Lin X, Zhang J, Chen L, et al. Tyrosine phosphorylation of Rab7 by Src kinase. *Cell Signal*. 2017;35:84–94.
92. Pollard SM, Yoshikawa K, Clarke ID, et al. Glioma stem cell lines expanded in adherent culture have tumor-specific phenotypes and are suitable for chemical and genetic screens. *Cell Stem Cell*. 2009;4(6):568–580.
93. Gump JM, Dowdy SF. TAT transduction: the molecular mechanism and therapeutic prospects. *Trends Mol Med*. 2007;13(10):443–448.
94. Dozio V, Sanchez J-C. Profiling the proteomic inflammatory state of human astrocytes using DIA mass spectrometry. *J Neuroinflammation*. 2018;15(1):1–14.
95. Vujić T, Schvartz D, Furlani IL, et al. Oxidative stress and extracellular matrix remodeling are signature pathways of extracellular vesicles released upon morphine exposure on human brain microvascular endothelial cells. *Cells*. 2022;11(23).
96. Teo G, Kim S, Tsou CC, et al. mapDIA: preprocessing and statistical analysis of quantitative proteomics data from data independent acquisition mass spectrometry. *J Proteomics*. 2015;129:108–120.
97. Team RC. *R A Language and Environment for Statistical Computing*. Vienna: R Foundation for Statistical Computing; 2021. - References - Scientific Research Publishing https://www.scirp.org/(S(i43dyn45teexjx455qlt3d2q))/reference/ReferencesPapers.aspx?ReferenceID=1787696.
98. Perez-Riverol Y, Csordas A, Bai J, et al. The PRIDE database and related tools and resources in 2019: improving support for quantification data. *Nucleic Acids Res*. 2019;47(D1):D442–D450.